Aus dem Institut für Laboratoriumsmedizin der

Ludwig-Maximilians-Universität München

Vorstand: Prof. Dr. med. D. Teupser

Intravascular immunity against systemic bacterial infection and metastasis

Dissertation

zum Erwerb des Doktorgrades der Humanbiologie

an der Medizinischen Fakultät der

Ludwig-Maximilians-Universität zu München

vorgelegt von

Manovriti Thakur

aus

Himachal Pradesh, Indien

2019

Mit Genehmigung der Medizinischen Fakultät

der Universität München

Berichterstatter: Prof. Dr. med. Bernd Engelmann

Mitberichterstatter: Priv. Doz. Dr. rer. nat. Wolfgang Fischer

Prof. Dr. Hans-Joachim Stemmler

Mitbetreuung:

Dekan: Prof. Dr. med. dent. Reinhard Hickel

Tag der mündlichen Prüfung: 03.07.2019

Abbreviations

Ab/α	Antibody
AMPs	Antimicrobial peptides
α-2AP	Alpha 2-antiplasmin
BSA	Bovine serum albumin
C monocytes	Classical monocytes
Ca	Calcium
CFUs	Colony forming units
CLR	C-type lectin receptors
DAMPs	Damage-associated molecular patterns
DNA	Deoxyribonucleic acid
DMEM	Dulbecco's Modified Eagle's medium
EVs	Extracellular vesicles
FACS	Fluorescence-activated cell sorting
FDPs	Fibrin degradation products
FMO control	Fluorescence minus one control
FpA	Fibrinopeptide A
FpB	Fibrinopeptide B
GFP	Green fluorescent protein
LSM	Laser scanning microscope
MV	Microvesicles
MACS	Magnetic-activated cell sorting
NC monocytes	Non classical monocytes
NEAA	Non-essential amino acids
NLRs	NOD-like receptors
NOD	Nucleotide oligomerization domain
NKT cells	Natural killer T cells
NETs	Neutrophil extracellular traps
PAI-1	Plasminogen activator inhibitor-1
PAI-2	Plasminogen activator inhibitor-2
PAMPs	Pathogen-associated molecular patterns

PBMCs	Peripheral blood mononuclear cells
PBS	Phosphate buffer saline
PLG	Plasminogen
PRRs	Pattern Recognition Receptors
ROS	Reactive oxygen species
STED	Stimulated emission depletion
SEM	Scanning electron microscope
TAMs	Tumor-associated macrophages
TAFI	Thrombin activatable fibrinolysis inhibitor
TEM	Transmission electron microscopy
TEG	Thromboelastography
TF	Tissue factor
TFPI	Tissue Factor Pathway Inhibitor
TLR	Toll-like receptor
tPA	Tissue-type plasminogen activator
uPA	Urokinase-type plasminogen activator
uPAR	uPA receptor
WT	Wild type

Contents

I. Introduction

I.1. Systemic bacterial infection

Circulating bacteria, viruses or fungi can cause systemic infections. The infections trigger the innate intravascular immune system through pattern recognition receptors (PRRs) that recognize microbial components; so-called pathogen associated molecular patterns (PAMPs) and biomolecules from damaged tissues termed damage-associated molecular pattern molecules (DAMPs). PRRs are either cytoplasmic or membrane bound and consist of toll-like receptors (TLRs), nucleotide-binding oligomerization domain-(NOD) like receptors (NLRs) and c-type lectin receptors (CLRs)[1,2]. Altogether, they activate intravascular immune system. Sepsis represents a dysregulation of intravascular immunity as it is an unbalanced host response to a systemic infection which can lead to life threatening multi-organ failure. More than 30 million people are affected worldwide every year which causes 6 million deaths[3].

I.1.1. Intravascular immunity

Intravascular immunity consists of humoral and cellular components and plays an important role in clearance of bacteria or other pathogens from the circulation.

Humoral immune response. Humoral immune responses act through neutralization of pathogens by antibodies as produced by plasma cells and involves the binding of the antibodies to the pathogens as well as through activation on of the complement system.

Antibodies: Antibodies can coat the pathogen also known as opsonization, which consequently promote uptake of pathogen by phagocytic immune cells. Furthermore, binding of antibodies to the pathogen can also activate the complement system which can lead to lysis of microorganisms by introducing pores in their cell walls with the use of membrane attack complex[4,5].

Complement activation: The complement system is a major component of the immune system which leads to generation of C3a and C5a, also known as anaphylatoxins and contributes to opsonization of pathogens as well as chemoattraction of immune cells for the removal of apoptotic and necrotic host cells. The production of C3a and C5a has pro-inflammatory effects, which can enhance for example the recruitment of platelets, neutrophils and monocytes to the site of injury or inflammation.

C3a and C5a receptors have diverse roles in sepsis as C3a binds to macrophage C3a receptor can decrease the initial infection in a murine polymicrobial sepsis model and C5a receptor antagonist administration enhanced survival in the same model [6]. C5a signalling inhibition in various experimental studies using models such as Escherichia coli (*E.coli*) sepsis in baboons and abdominal sepsis in rats also suggested inhibitory effects of C5a in sepsis[7].

Cellular immune response. The cellular intravascular immune response acts through various immune cells including neutrophils, different types of monocytes, invariant natural killer cells (NKT), Kupffer cells and even endothelial cells which play important roles in the clearance of circulating bacteria and prevention of the bacterial dissemination to different organs via the blood stream**.**

Neutrophils and NETs formation: Neutrophils are innate phagocytic cells that are one of the first cells to arrive at sites of pathogen colonisation or vessel wall injury. They provide protection against pathogens via phagocytosis, generation of reactive oxygen species (ROS) and neutrophil extracellular traps (NETs) and others[8]. They can also increase vessel permeability and have an impact on coagulation cascade by interacting with platelets. Platelet-neutrophil conjugate formation promotes early activation of neutrophils which leads to degranulation, increased tissue factor expression and thereby stimulates thrombus formation[9]. Neutrophils can contribute to pathologic venous and arterial thrombosis or 'immunothrombosis' by the release of NETs. NET release is emerging as a major contributor to thrombus formation in many pathologic situations such as sepsis and malignancy[10,11].

NETs are large extracellular, web-like structures consisting of DNA, histones and serine proteases and embody strong microbicidal properties. Two processes initiate formation of NETs known as NETosis: the cell death pathway and non-lytic NETosis. The cell death pathway involves disassembly of nucleus, chromatin condensation and plasma membrane rupture. During non-lytic NETosis, granule proteins and nuclear chromatin get secreted and accumulate extracellularly[10]. Besides, residual anucleated cytoplast of the neutrophils it still continues to engulf microorganisms.

Monocytes: Monocytes are bone marrow derived circulating phagocytes which comprise 3-10% of leukocytes in humans and play a role in the cellular defence against pathogens, homeostasis and

tissue repair. Human monocytes are divided into 3 different subtypes in humans classical (C) ($CD14^{++}$, $CD16^{-}$), intermediate ($CD14^{+}$, $CD16^{+}$), and non-classical (NC) ($CD14^{+}$, $CD16^{++}$) monocytes. Murine monocytes are divided into two groups: C monocytes ($CD115^{+}$ $Gr1^{+}$) and NC ($CD115^{+}$ $Gr1^{-}$)[12,13].

C monocytes in humans comprise about 80–95% of circulating monocytes. These cells are highly phagocytic and are known to express a wide range of scavenger receptors. Intermediate monocytes comprise about 2–8% of circulating monocytes. Their functions include production of ROS, antigen presentation, support of the proliferation and stimulation of T cells, inflammatory responses, and angiogenesis. NC monocytes comprise about 2–11% of circulating monocytes. They are mobile in nature and crawl the endothelium in the search for injuries within the endothelial layer of blood vessels[14]. They can have proinflammatory functions as they secrete pro-inflammatory cytokines in response to infection.

Kupffer cells: In contrast to the other types of tissue macrophages they can engulf circulating bacteria or other pathogens directly from the blood stream. The pathogens get engulfed within the macrophages into membrane-bound vacuoles (phagosomes) which mature and are converted into a highly microbicidal organelle called phagolysosome[15,16]. Kupffer cells are resident macrophages which scan the foreign material transferred from the gastrointestinal tract via portal vein into liver vasculature. The specificity of phagocytosis induced by Kupffer cells also depends on opsonization of pathogens by antibodies and complement proteins[17].

I.1.2. Coagulation system and immunothrombosis

Coagulation system: Recent work shows that apart from the complement system and immune cell-mediated phagocytosis intravascular coagulation participates in the response to circulating pathogen. The coagulation system comprises of two main pathways; intrinsic pathway (contact pathway) and extrinsic pathway (tissue factor (TF) pathway), which both lead to formation of fibrin. The intrinsic pathway is directed by contact with negatively charged surfaces, with XII and involves kininogen, and pre-kallikrein. Other cofactors of the intrinsic pathway are factor XI (FXI), factor IX (FIX) and factor VIII (FVIII). The extrinsic pathway is initiated by TF (CD142 or thromboplastin) which is a membrane spanning glycoprotein and usually exposed on extravascular cells like fibroblasts, epithelial cells, pericytes TF is also upregulated on monocytes and most probably on endothelial cells under infectious and inflammatory conditions. During endothelial

wall injury TF gets access to the blood circulation and interacts with coagulation factor FVII/VIIa which together activate factor X to factor Xa. The extrinsic tenase complex then activates FIX (FIXa) as well as factor II (prothrombin)[18]. Both the intrinsic and extrinsic pathways together activate the prothrombinase complex. The prothrombinase complex consists of FXa, FVa, calcium and negatively charged phospholipid membranes. Activation of prothrombinase complex causes the activation of the inactive zymogen prothrombin (factor II) to thrombin (factor II a). Thrombin then converts fibrinogen to fibrin and activates in a positive feedback loop factor XI, factor VII and as well as creates positive feedback for factor XIII.

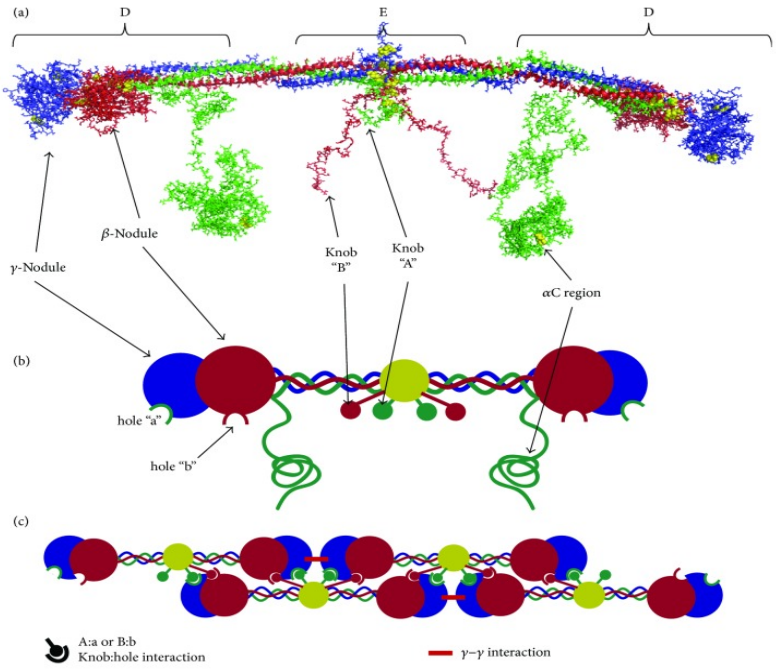

Figure 1: Structure of the fibrin molecule. (a) The fibrin structure has α chains; in green, β chains; in red, and γ chains; blue, disulphide bonds are emphasized as yellow spheres. Fibrin degradation fragments D and E are highlighted. Fragment X is formed from plasmin cleavage of the αC region. (b) Cartoon fibrin molecule: upon release of FpA and FpB by thrombin, knob A and knob B are exposed to bind the respective hole a and hole b. (c) Interaction of two fibrin molecules[23,24].

Thrombin converts fibrinogen to fibrin monomers by removal of the N-terminal fibrinopeptides A and B. The N- and C- terminals of these monomers join at E and D nodules, respectively. Fibrinopeptide A induces protofibril formation and hence helps in the aggregation of fibrin fibers (Fig. 1). During this aggregation, the E domain of one homodimer interacts with the D domain of

a second homodimer. This leads to the formation half of staggered fibrin threads within the thrombus[19].

Factor XIIIa (FXIIIa) enhances the cross linking of fibrin at lysine residues and increase the stability of fibrin clots[20]. The interaction of fibrin with different immune cells can also influence the clot density and its mechanical properties. For instance, incorporation of platelets into fibrin scaffolds lead to compact and more stiff clot. Platelet and fibrinogen together can act as an active surface for the recruitment, attachment and activation of neutrophils or other phagocytic cells [21,22].

Immunothrombosis. Microvascular fibrin formation, platelet and neutrophil recruitment, NET formation, as well as the activation of TF-positive monocytes at the site of pathogen adhesion during systemic infection can lead to immunothrombosis. One study where intravascular thrombosis was inhibited by using TF antagonist TFPI suggests that immunothrombosis is highly influenced by microvascular coagulation [25].

Microvascular coagulation and its ability to promote immunothrombosis were found to entrap circulating bacteria, inhibit their invasion into perivascular tissue or to other tissues and induce killing of pathogens. Immunothrombosis might perform the bacterial killing by providing a platform for antimicrobial peptides as well as serine proteases like NE [26]. However, uncontrolled immunothrombosis can induce excessive inflammatory response inside blood vessels during sepsis, which is known as disseminated intravascular coagulation[27].

I.1.3. Fibrinolysis

Fibrinolysis is defined as the breakdown of fibrin clots by plasmin either on the thrombus surface or on cells expressing fibrinolytic receptors. Plasmin acts on C- domains in fibrin, removing a peptide bond from the N terminal domain of the b-chain and to cleave the coil connector of E and D- domains[28] (Fig. 2).

Plasmin is activated from its zymogen form plasminogen (PLG) by the action of two serine proteases: tissue plasminogen activator (tPA) and urokinase plasminogen activator (uPA). tPA is mostly produced by endothelial cells and uPA is synthesized by monocytes, macrophages and some epithelial cells [29]. The enzymatic activity of tPA increases by 2 fold when present together with fibrin and PLG. On the other hand, uPA does not require fibrin as it acts directly on the open conformation of PLG [30], [31].

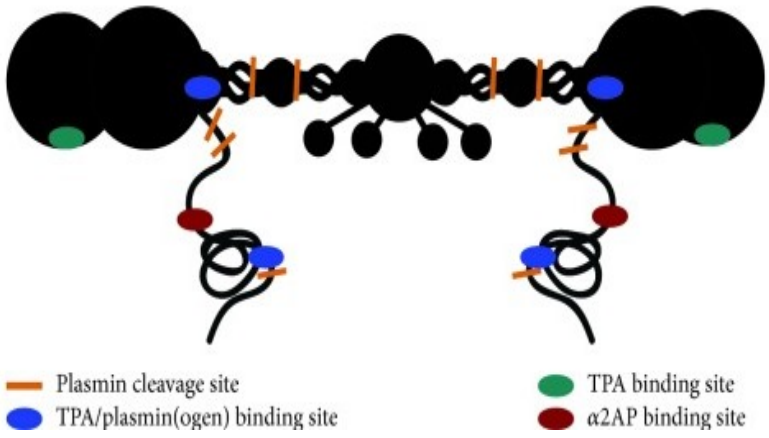

Figure 2: Fibrin fiber structure showing fibrinolytic binding and cleavage sites. Relative positions of plasmin cleavage sites, and tPA, PLG and *α*2AP binding sites are color coded[23].

uPA and tPA can be inhibited by plasminogen activator inhibitor-1 (PAI-1) (Fig. 3)

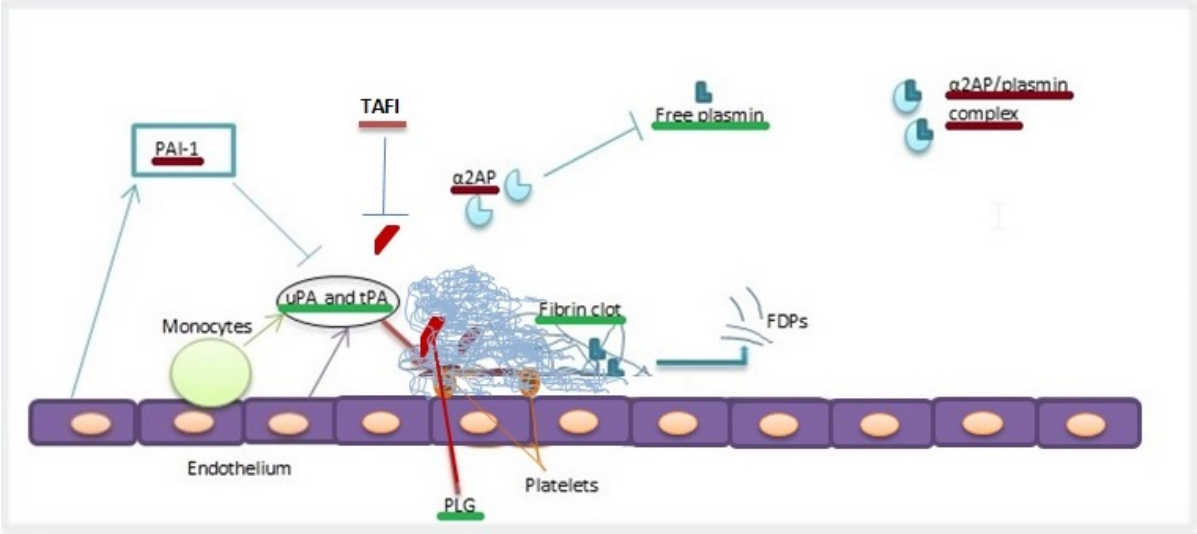

Figure 3: Fibrinolysis and its inhibitors. uPA and tPA secreted from immune cells and endothelial cells, respectively, act on PLG and generate plasmin which in turn degrades fibrin to form fibrin degradation products (FDPs). α2AP, PAI-1 (red) together with TAFI act as main inhibitors of fibrinolysis.

In addition, plasmin activity is controlled by circulating inhibitors like α2-antiplasmin (α2AP) and plasminogen activator inhibitor-2 (PAI-2). Fibrinolysis can also be counter regulated by thrombin activatable fibrinolysis inhibitor (TAFI). TAFI acts by removing C-terminal lysine and arginine from fibrin thus influencing the binding of plasminogen to fibrin [32] .

I.2. Immune response to tumor cells and their extracellular vesicles (EVs)

Intravascular immunity not only responds to pathogens but also responds to circulating tumor cells and their vesicles. Hence, intravascular coagulation could be also triggered by tumor structures in the microcirculation.

I.2.1. EVs

EVs are membrane bound particles which consists of various subtypes, including exosomes (50-100 nm) formed via endosomal pathway, microvesicles (MVs) (0.1- 1μm) as a result of plasma membrane budding, and large oncosomes (1-10 μm) released by proliferating cancer cells. EV cargos appear to control basic cellular functions, communication between immune cells as well as the pathogenesis of multiple diseases like cancer [33].

I.2.2. MVs and metastasis

Unlike exosomes, MVs originate directly from plasma membrane of all cell types and are released via actin -myosin-driven fission into the extracellular space. MVs can establish cell-cell communications by transferring their cargoes, like proteins and microRNAs to the target cell, thereby modulating cellular functions even to distant regions of body. Differences in MV cargos are highly dependent on the cells where MVs originate from[34].

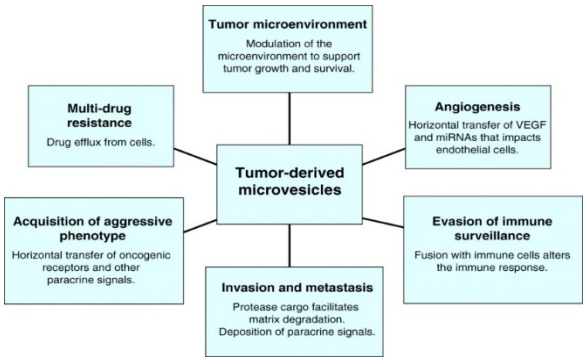

Figure 4: Tumor MVs and their various functions[35].

MVs are released under physiological conditions while excessive release of MVs is known to occur under pathological conditions. Notably, increased levels of MVs have been described in patients with different types of metastatic cancer. Tumor derived MVs have been proposed to participate in

enhancing tumor cells migration, angiogenesis, blood coagulation, tumor growth, extracellular matrix degradation and metastasis (Fig.4) [35].

I.2.3. Intravascular immune system and metastasis

Immune cells play an important role in identifying and killing circulating cancer cells, cell debris or their microvesicles. CD8+ T cells and natural killer (NK) cells are known to be cytotoxic for metastatic tumor cells[36, 37]. Yet, tumor cells can manage to escape from the immune system and to extravasate[38]. Immunosuppression by tumor cells can be mediated by secreting immunosuppressive cytokines like IL-10 and TGF-β [39]. Classical monocytes in mouse are also capable of promoting tumor growth [40].

Macrophages, because of their plasticity tend to actively participate in metastasis. Tumor cells can manipulate anti-metastatic immune cells to become pro-metastatic as best demonstrated for tumor associated macrophages (TAMs). TAMs are most abundant cells in tumor microenvironment can secrete immunosuppressive cytokines. These immunosuppressive cytokines and chemokines could suppress $CD4^+$ and CD 8^+ cells directly as well as indirectly by recruiting Tregs. TAMs can also negatively influence T cell activity by depleting L-arginine in the tumor environment [41, 42].

The role of tumor MV in tumor metastasis is still largely undefined. In particular it is unknown how they interact with intravascular immune cells and whether they can perform immune escape on the parent cells.

I.3. Objectives of study

Intravascular immunity aims to restrict bacterial survival and dissemination during systemic bacterial infection. Microvascular coagulation is likely a major component of intravascular immunity. However, crucial aspects of intravascular coagulation during systemic infection are still unknown. Hence, in the present study the following points were assessed:

- Immune cell recruitment implicated in microvascular coagulation during systemic bacterial infection.
- Mechanisms of cellular and molecular counterregulation of microvascular thrombosis.
- Role of T helper cells and NC monocytes during intravascular immunity.

In its second part, this study deals with influence of pancreatic tumor MVs on the metastatic potential of pancreatic cancer cells as influenced by intravascular immunity. To understand the correlation between tumor MVs, immune cells and metastasis in detail, the following questions have to be addressed:

- How do circulating tumor MVs interact with intravascular immune cells?
- How do circulating tumor MVs extravasate and contribute to progression of metastasis?

II. Material and methods

II.1. Material

II.1.1. Equipment

Equipment	Manufacturer
Balance MC1 LC 620 S	Sartorius (Göttingen, Germany)
Cell culture incubator	Binder GmbH (Tuttlingen, Germany)
Cell culture microscope	Carl Zeiss (Jena, Germany)
Count chamber Neubauer Improved	Brand (Wertheim, Germany)
Culture Hood	Heraeus
ELISA Reader Dynatech MR7000	Dynatech Laboratories
UV LED laser	Dymax
Incubator (cell culture)	Heraeus (Hanau, Germany)
Lamin Air flow HLB 2472	Thermo Scientific (Braunschweig, Germany)
Light microscope Axiovert 100	Zeiss (Jena, Germany)
LSM 510 Meta	Zeiss (Jena, Germany)
Mega centrifuge	Heraeus, Omnifuge 2.0 RS
Micropipettes (10µl, 20µl, 100µl, 200µl, 1000µl)	Eppendorf (Hamburg, Germany)
Multiphor II blotting device	Amersham Pharmacia Biotech
Nano Drop	Thermo Fisher Scientific (Schwerte, Germany)
pH meter	HANNA instruments (Quebec, Canada)
Pipet boy	Integra-Bioscience (Biebertal, Germany)
Pippets (5ml, 10ml)	Omnilabs GmbH Co. KG (Bremen, Germany)
Fortessa	BD Biosciences
Thermocycler	Biozyme, MiniCyclerTM, MJResearch
Thrombelastograph	RoTEG Dynabyte GmbH
Vortexer	Sartorius (Göttingen, Germany)
Water bath Julabo U3	Julabo Labortechnik (Allentown, USA)
2 Photon	LaVision BioTec GmbH (Bielefeld, Germany)

II.1.2. Reagents and chemicals

Substance	Manufacturer
Ampicillin sodium salt	Sigma-Aldrich Chemie GmbH, Steinheim, Germany
Bovine Serum Albumin (BSA)	Sigma-Aldrich Chemie GmbH, Steinheim, Germany
Dako Pen	Dako Denmark, Glostrup, Denmark
DAPI (4',6-diamidino-2-phenylindole)	Thermo Fisher Scientific, Carlsbad, USA
Ethanol denatured 99.8 %	Carl Roth GmbH + Co. KG, Karlsruhe, Germany
FACS Buffer	BD Biosciences
Glycerol	Merk millipore
KCl (Potassium chloride)	Merck, Darmstadt, Germany
KH_2PO_4 (Potassium dihydrogen phosphate)	Carl Roth GmbH + Co. KG, Karlsruhe, Germany
NaCl (Sodium chloride)	Carl Roth GmbH + Co. KG, Karlsruhe, Germany
Na_2HPO_4 * 2 H_2O (di-Sodium hydrogen phosphate dihydrate)	Carl Roth GmbH + Co. KG, Karlsruhe, Germany
Paraformaldehyd (PFA)	Carl Roth GmbH + Co. KG, Karlsruhe, Germany
Sucrose	Sigma-Aldrich Chemie GmbH, Steinheim, Germany

II.1.3. Antibodies

Antibody	Conjugation	Concentration	host	Source
CD4 (Ultra-LEAF)	-	7 µg/ml	rat	Biolegend
CD2	PE	1:100	rat	Biolegend
CD14	PacBlue	1:50	rat	Biolegend
CD16	PE-Cy7	1:50	rat	Biolegend
CD15	PE	1:50	rat	Biolegend

CD19	PE	1:50	rat	BD Biosciences
CD36	-	3mg/kg	rabbit	BD Biosciences
CD56	PE	1:100	rat	Biolegend
CD335	PE	1:100	rat	Biolegend
CX3CR1	-	1:100	rabbit	Novus Biologicals
E.coli LPS	-	1:200	mouse	Abcam
E.coli LPS	PE	1:100	mouse	Self labelled
F4/80	-	1:100	rat	Abcam
F4/80	-	1:400	rat	Biolegend
Fibrin	-	1:100	mouse	WAK
GFP	-	5 µg/ml	rabbit	Abcam
HLA-DR	FITC	1 µl/50 µl	rat	Biolegend
LC3	A550	0,4 µg/ml	rabbit	Novus
Ly6C	A488	1:400	rat	Thermofischer
Ly6C	-	1:400	rat	Thermofischer
Ly6G	-	15 µg/ml	rat	BD Biosciences
mouse IgG	A594	2 µg/ml		Thermofischer
RORγT	-	1:100	rabbit	Biorbyt
Stabilin 2	-	5 µg/ml	Mouse	Kai Schledzewski
Stabilin 2	PE	7 µg/ml, 10 µg/ml	mouse	Self labelled
T-bet	-	1:100	rabbit	Antibodies-online
tPA	-	1:100	rabbit	GeneTex
uPA	-	1:100	goat	GeneTex
uPAR	-	1:400	goat	R&D

II.1.4. Buffers

<u>$CaCl_2$ (Faktor Xa Formation; 50ml)</u>

225 mg $CaCl_2 .2H_2O$

ddH_2O

Ca/Hepes (TEG)

10 mM Hepes

100 mM $CaCl_2$,

ddH_2O, pH 7.4

PBS (Phosphate Buffered Saline) (1L)

8 g NaCl

0.2 g KH_2PO_4

1.42 g $Na_2HPO_4.2H_2O$

0.2 g KCl

Permabilisation/ Blocking-Buffer

0.2 % Fish Skin Gelatin

0.5 % BSA

0.1 % Saponin

TNC (Tri-Nitrium Citrate for blood drawing)

3.68 g TNC

100 ml H_2O

Blocking buffer

1.5g BSA

100 ml ddH_2O

Sterile filtered

Resuspension buffer (1L)

138 mM NaCl

2.7 mM KCl

12 mM NaHCO3

0.4 mM NaH2PO4

1 mM MgCl2.6H2O

5 mM D-Glucose

5 mM Hepes

pH 7.35

II.1.5. Bacteria and cell lines

Type	Origin	Source
L3.6pl	Human pancreatic cancer cell line	Prof. Christiane Bruns, Klinik für Allgemein-Viszeral- und Gefäßchirurgie, Köln, D
KCP	Mouse pancreatic cancer cell line	Dr. Hana Algül, II. Medizinische Klinik und Poliklinik, Klinikum rechts der Isar der TU München (München, D)
THP1	Human	DSMZ ACC 16, Deutsche Sammlung von Mikroorganismen und Zellkulturen GmbH (Braunschweig, D)

II.1.6. Mouse models

Type/ Name	Source
C57BL/6	Charles River
Kaede-tg mice	Prof. Samuel Huber, I. Medizinische Klinik und Poliklinik, UKE Hamburg, D
CX3CR1-eGFP	Prof. Steffen Massberg, Medizinische klinik und Poliklinik I., Klinikum der Universität, München, D
UPAR-/-	Prof. Karen Vanhoorelbeke, Kulak Kortrijk Campus, KU Leuven, Belgium
PLG-/-	Prof. Karen Vanhoorelbeke, Kulak Kortrijk Campus, KU Leuven, Belgium

II.2 Methods

II.2.1. Preparation of bacteria

E.coli K12 strain used in all experiments was GFP (green fluorescent protein) labelled and was grown overnight in 50 ml falcons with LB-medium and 100 µg/ml ampicillin. Next day the mixture has been centrifuged at 4000 rpm for 10 min and optical density (OD) was measured at 600 nm to estimate the bacterial number. For animal injections $3.2x10^8$ bacteria were used.

II.2.2. Animal experiments

WT mice were usually obtained from Charles River and treated as per the guidelines of the local legislation on animal protection (Regierung von Oberbayern, Munich). The experiments were performed under pathogen free conditions at the animal facility of Walter Brendel Center. Some animal experiments were done at the animal facility of KU Leuven Kulak, Belgium and UKE Hamburg.

The animals were infected with $3.2x10^8$ *E.coli* via tail veil injection and the organs (liver, spleen, lung, kidney, heart, brain) and blood were collected after different time points (1 hr, 3 hr, 6 hr, 24hr, and 48hr).The injection schemes for all the animal experiments are as follows:

Scheme 1: WT mice, Infection model

0hr ---------- 1hr/3hr/6hr/24hr/48hr
E.coli injection ---------- sacrifice and organ collection.

0hr----------2hr---------- 7hr
Anti-MIF ab----------*E.coli* injection---------- sacrifice and organ collection.

0hr----------4hr----------7hr
DNase1----------*E.coli* injection---------- sacrifice and organ collection.

0hr----------24hr----------27hr/30hr
CD4 ab----------*E.coli* injection---------- sacrifice and organ collection.

Scheme 2: (Knock-outs)

0hr----------3hr/6hr/18hr/24hr

E.coli injection (tail vein) ----------x

Scheme 3: (Kaede mice)

0hr----------12hr----------3hr/6hr

Photoconversion ---------*E.coli* injection----------x

To investigate the microvascular coagulation and the immune cell recruitment neutralizing antibodies or proteins were administered before *E.coli* injections at time points 0 hr, 2 hr, 4 hr and 24 h. *E.coli* was injected at various time points as shown in the schemes and animals were sacrificed after 1-24 hr post infection.

Kaede mice have photoconvertible fluorescence protein that changes from green to red upon exposure to UV light. These mice were submitted to surgery proceed for the small intestine exposition to photoconvert Th17 cell population in the small intestine. The small intestine was exposed to UV light by using Dymax LED UV laser for 1 min three times. After 24 hrs of surgery, *E.coli* was injected and organs were harvested at 3 hr or 6 hr post infection from these animals. Small part of each organ was kept in separate eppicups for CFU analysis and rest of the organ was fixed in 2% paraformaldehyde solution for 2 hr. The fixed organs were then transferred to 30% sucrose solution (to preserve GFP signal from Labelled bacteria) incubated overnight at 4˚C after which the organs were stored at -80˚C.

II.2.3. CFUs

After sacrificing the mouse, small part of each organ was weighed, homogenized in PBS with scalpel and then transferred to 15 ml falcon tubes with glass beads and 1ml PBS. The number of viable bacteria in the homogenates of organs was determined by plating 10 fold serial dilutions on LB plates. For liver and spleen, 1:100, 1:1000 and 1/10000 dilutions were made whereas, for all other organs 1:10 and 1:100 dilutions were made. Plates were stored at 37 ˚C overnight and CFUs were counted as amount per gram weight of organ.

II.2.4. Immunostaining of cryosections

The organs were stored for at least 24 hr at -80˚C and then embedded in tissue tek at -20˚C inside the cryotome. Frozen sections were made ranging from 5 µm to 10 µm and collected on super frost glass slides. Cryosections from mouse liver were fixed in 4% PFA for 10 min, washed with PBS (3 times, 3 min each), blocked/permeabilized with 0.1% Triton X/1.5% bovine serum albumin (BSA) solution in PBS for 40 min and washed again. Unlabelled or labelled primary antibody was added to slides and incubated overnight. Next day after washing the slides were incubated with secondary antibody if required (2 µg/ml, 1 hr, 4˚C).

In some cases, staining was done using macrophage-specific anti-F4/80 antibody (10 µg/ml; Abcam), followed by staining with Alexa546-labeled secondary antibody (2 µg/ml, Thermo Fisher Scientific). Sinusoids were labeled with Alexa488-primary labeled anti-stabilin2 antibody (5 µg/ml; InVivo BioTech Services). The sections were mounted in Vectashield® with DAPI (Vector Laboratories) and analyzed by confocal microscopy. In other experiments, pre-metastatic clusters of tissue cells were counted at different time points (day 4, day 8 and day 14), and were defined as groups of at least 6 nuclei at a distance of < 2 µm from each other. For each experiment 10 randomly chosen consecutive visual fields were analyzed. Two methods of detections were used: (i) direct immunostaining wherein the antigen is directly detected by a primary antibody coupled with a fluorophore and (ii) indirect immunostaining in which case the antigen is detected by a primary antibody, which is in turn detected by a secondary antibody coupled with fluorophore. Draq5 or DAPI were used to stain the nucleus. The slides were then washed, mounted with glycerol and analysis was performed using confocal laser scanning microscope from Zeiss.

II.2.5. Isolation of human monocytes via MACS

All experiments with human blood donor were approved by the ethics commission of the medical facility of LMU. Blood from healthy donors was obtained and drawn into 20 ml syringe with 2 ml tri-sodium citrate solution and 13 µl hirudin solution. Blood was then transferred into centrifugation tubes and centrifuged at 1,300 rpm for 15 min without brake at room temperature (RT). The plasma was removed and the buffy coat diluted 1:2 with monocyte wash buffer. 50 ml Falcons were filled with 15 ml ficoll, the diluted buffy coat was layered on top and centrifuged at 380 g for 25 min without break at RT. The middle layer containing the cells was isolated into 50 ml

Falcons and filled up to 30 ml with monocyte wash buffer. The falcons were centrifuged at 320 g for 10 min without brake at RT. The supernatant was decanted and the pellet was resuspended in a volume of 500 µl antibody wash buffer with anti-CD14 Microbeads (Miltenyi, 1 µl/ml blood). The cells were incubated for 15 min at 4 °C, during this time the column was placed in a magnet and was equilibrated with 500 µl antibody wash buffer. The cell suspension was diluted with another 500 µl antibody wash buffer and applied to the column. The column was washed two times with antibody wash buffer and then removed from the magnet. The positive fraction was eluted with 1 ml antibody wash buffer by pressing down with the stamp. The cells were pelleted at 320 g for 10 min without brake at RT. The cells were resuspended in resuspension buffer and counted.

II.2.6. Isolation of human monocytes via FACS

PBMCs were isolated in the same way as explained using the ficoll method and then resuspended in FACS buffer. The cells were divided into two parts; one part is used for all the single stains, unstained and FMO controls while the other half was used as a sample for sorting. Single stains used for lineage control included αCD335, αCD3, αCD56, αCD19 and αCD15. Controls for CD16 and CD14 were stained with αCD16 and αCD14 respectively. HLA-DR control was stained with HLA DR antibody was used (Fig. 5).

Gating strategy:

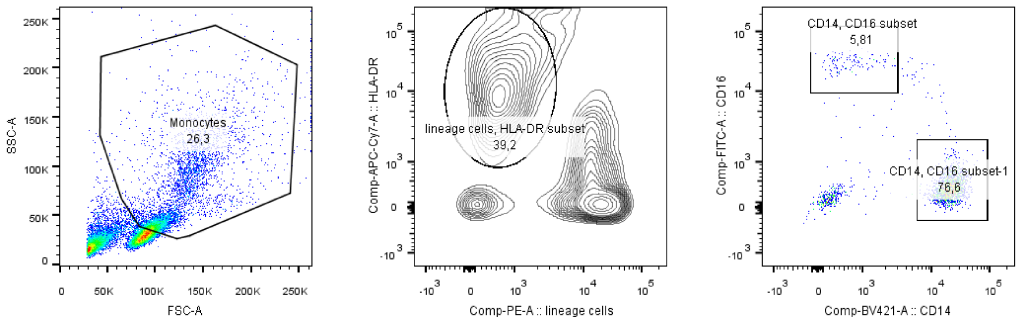

Figure 5: Gating strategy used for isolation of monocyte subsets from human blood. Negative selection was done to exclude lineage cells in the total population and only HLA-DR subset was gated. From these subsets CD14 and CD16 cells were gated and isolated.

The FMO CD16 control had all the above-mentioned antibodies except αCD16 and FMO CD14 control also had all the antibodies except αCD14. In the sample we had all the antibodies. All the samples were incubated for 15-20 min and then washed twice at 350 g for 7 min, followed by

resuspension in FACS buffer. C monocytes were stimulated by using LPS (100 ng/ml for 2.5hr) and NC monocytes were stimulated using ORN R-0006-TLR7/8 agonist for 2.5hr and thereby used for various assays.

II.2.7. Isolation of mouse Th17 cells

The liver was cut into tiny pieces and put in to 15 ml tube containing 6 ml of collagenase buffer for 45 min at 37°C. After the collagenase incubation the liver was smashed with metal strainer, washed with PBS/1% FBS, followed by centrifugation at 1,600 rpm for 10 min. The pellet was resuspended in 4 ml 40% Percoll, laid carefully on top of 4 ml 67% Percoll and centrifuged at 400 g for 20 min, (room temperature) with slow acceleration. After centrifugation, the T cells were taken out by a 1 ml pipet from the interphase and transferred into 50 ml falcon tubes. The falcon tubes were then centrifuged at 1500 rpm for 5 min and resuspended in PBS/1% FBS followed by cellular staining by FACS. First lymphocyte population was gated; second doublets were removed by using FSC-H and FSC-W. After setting gate 3 for Foxp3 positive and IL17a cells, in the next gate CD3 and CD4 positive cells were selected. In the next step, CD4 positive cells having expression of IL-17a were isolated. These cells define Th17 cells, which could further be isolated as anti-inflammatory or Pro- inflammatory Th17 phenotypes (Fig. 6).

In some cases, the naïve CD4 positive cells and APCs were isolated from peripheral lymph nodes and spleen of mice followed by their differentiation to anti-inflammatory or pro-inflammatory Th17 cells. Peripheral lymph nodes and spleen were isolated and smashed through 100 µm strainer. Followed by washing with FACS buffer and spun down at 1500 rpm for 5 min. Magnetic sorting was performed with the pellet. Negative selection was performed using anti-CD25-biotin and anti-CD44-biotin antibody, 15 min incubation on ice and spun down. Then streptavidin beads (40 µl beads/ml) were added and incubated for 30 min. Next, the suspension of cells was put through the MACS column which was previously hydrates and washed 3 times. Before the suspension was put on the column, it has to be filtered out using 45 µm strainer to avoid the collapse of the column. The eluted solution is CD4 positive cells, which again were incubated with CD4-streptavidin magnetic beads (100 µl/ml) for 30 min. Eluted solution had CD4 negative population and in the column was CD4 positive cell population. CD4 positive cells were then spun down and added to the 12 well plate with medium. For the APCs, CD3 selection was performed. CD4 negative

population was then incubated with CD3 magnetic beads (15 min) and the loaded to MACS column. The eluted population was rich in APCs.

For differentiation, we have used CD4 positive cells (13 x 10^6 cells), APCs (32 x 10^6 cells) and specific cocktails. For pathogenic Th17 cells we used αCD3 (3 µg/ml), αCD28 (1 µg/ml), IL1B (10 ng/ml), IL6 (10 ng/ml), IL23 (20 ng/ml), αINFγ (10 µg/ml) and IL4 (10 µg/ml).

However, for anti-inflammatory Th17 cells, different cocktail was used which contained αCD3 (3 µg/ml), TGF-β (1ng/ml), IL6 (10 ng/ml), FICZ (100nM), αINFγ (10 µg/ml) and IL4 (10 µg/ml). After 3-5 days, the proliferation was checked and cells were gated in the FACS sorter for CD4 and IL17a positivity.

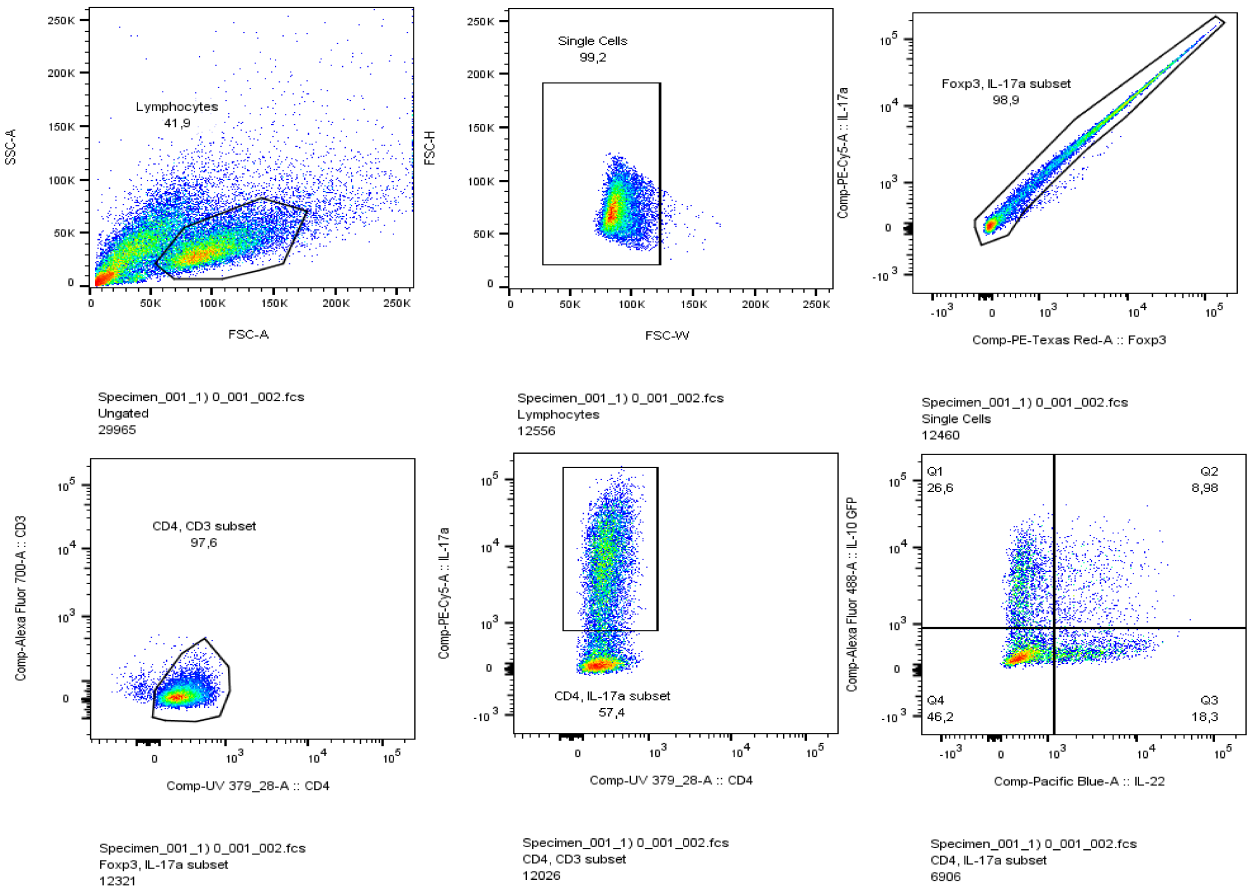

Figure 6: Gating strategy for isolation of Th17 cells from mouse lymphoid organs and spleen. First lymphocytes were gated from the whole population followed by single cell gating. Secondly, CD4, CD3 subsets were gated to make sure they are not innate T cell subsets. Last gate was introduced to choose CD4 and IL17a positivity on cells which represent Th17 cell subsets.

II.2.8. FACS analysis

T cells were isolated from livers of *E.coli* infected and from non-infected Kaede mice, 3 hr post infected and 6 hr after infection using the same Percoll gradient as mentioned in the section II.2.7.

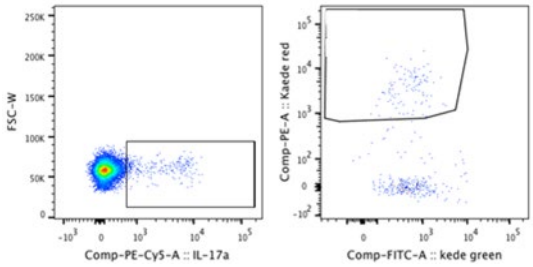

Figure 7: Gating strategy used for analysis the translocation of Kaede photoconverted Th17 cells from small intestine into the liver and the lung.

II.2.9. FXa formation assay

To measure the procoagulant activity of different immune cells we performed a chromogenic assay detecting the generation of factor Xa. Once factor X gets activated to factor Xa, there is a colour change due to cleavage of chromogenic substrate S2222. Serial dilutions of the standard Thromborel-S (CSL Behring) were prepared followed by addition of 50 µl $CaCl_2$ to each well of a 96-well plate. Then to these wells 50 µl of standard or samples were added. A master mix of chromogenic substance S-2222, Beriplex (CSL Behring) and respective amount of resuspension buffer was prepared such that 100 µl of this mix could be pipetted into each well. The absorption was measured at 405 nm using a plate reader (softMAXpro). A cycle of 6 min was repeated for a total of 36 min and the final values were expressed as mU/ml.

II.2.10. Thromboelastography (TEG)

The procoagulant activity of different monocyte subsets in whole blood was analyzed using thromboelastography. The assay was performed in a specialized TEG pin and cup apparatus. To 250 µl of whole blood 60 µl of solution of 30 mM $CaCl_2$+ HEPES and 30 µl of sample (10,000 cells of each monocyte subset) was added in each cup. Directly after, the coagulation will start and therefore the measurement needs to be started immediately. The whole TEG preparation needs to be done very carefully and fast, to get as reliable and best results as possible, because the TEG is very sensitive. The most important parameter of the clotting, given by the TEG, is for the current experiments the Clotting Time (CT). The CT-value is the time from the reaction start until the fibrin formation starts. Additionally, the Clot Formation Time (CFT) is given, showing the time

from the beginning of fibrin formation until the time when the clot has a size of 20mm. The Maximal Clot Firmness (MCF) stands for the maximum firmness of the clot in mm and the TEG can give the amplitude reached after 10 min (A10) and the respective times when those parameters are reached. When the measurement runs long enough, fibrinolysis can also be shown, for example via the Lysis Index 30 minutes after CT (LI 30) or the Maximal Lysis (ML) and the respective time.

II.2.11. Plasmin activity assay

To analyze the fibrinolytic activity of different immune cells a plasmin activity assay was performed. First a clot was prepared in 96 well plates with the use of 20 µl thrombin (4 U/ml), 60 µl fibrinogen-plasminogen mix (fibrinogen 2.5 mg/ml and plasminogen 1 mg/ml), incubating it for 37 min at 37°C. Afterwards chromogenic substrate of S-2251 (1.5 mmol/L) and immune cells were added and the O.D was measured every 10 minutes for 1 hr at 405 nm to check for the protease activity of plasmin associated with immune cells.

II.2.12. Quantitative polymerase chain reaction

RNA isolation: Isolated immune cells (stimulated or unstimulated, 10^7 cells) were lysed by resuspension in TRIzol (600 µl) and processed for RNA purification. RNA isolation was performed using the Direct-Zol RNA miniPrep Plus kit (Zymo Research). After following the instructions from the manufacturer the isolated RNA was stored in RNase/DNase free tubes at -80°C.

First strand cDNA synthesis: cDNA synthesis has performed using 800 ng of total RNA and 1 µl of random hexamer primers. The mixture was incubated at 65°C for 5 min. After incubation the vial was transferred to ice. 4 µl of 5X Reaction Buffer, 1 µl of RiboLock RNase Inhibitor (20 U/µl), 2 µl of 10 mM dNTP Mix and 1 µl of RevertAid M-MuLV RT (200 U/µl) were mixed in the indicated order and added to the RNA-mix, giving a total volume of 20 µl per sample. The vial was then heated up to 25°C for 5 min, followed by 60 min at 42°C, finally yields cDNA.

qPCR amplification of first strand cDNA: The cDNA was diluted 1:10 with nuclease free water. A mix of 2.5 µl Premix Ex Taq Master Mix and 0.5 µl Sonda Taqman was prepared and added upto final volume of 3 µl in each well of a microplate. 2 µl of the diluted cDNA was added to the wells, giving a total volume of 5 µl per well. Analysis of qPCR QuantStudio Software V1.2 was used. All experiments were done in triplicates.

II.2.13. Two –photon intravital imaging

Two-photon intravital imaging was used to image in real time the engulfment of *E.coli* and fibrin debris by CX3Cr1 GFP^+ cells in liver sinusoids. Imaging was done using a multiphoton LaVision Biotech (Bielefeld, Germany) TrimScope II system connected to an upright Olympus microscope, equipped with a Ti:Sa Chameleon Ultra II laser (Coherent) tuneable in the range of 680 to 1080 nm. Additionally, an optical parametric oscillator compact (OPO) connected to the laser was giving extended wavelength with the range of 1000 to 1600 nm, for the far-red dyes excitation. An objective 16 × water immersion (numerical aperture 0.8, Nikon) was used. Single images were acquired from 80 µm to 100 µm depth, with z-interval of 2 µm. 820 nm was used as an excitation wavelength, with 1024×1024 pixels and detected by PMTs (G6780-20, Hamamatsu Photonics, Hamamatsu, Japan). ImSpector Pro (LaVision) was used as acquisition software. An environmental box maintained a stable 37°C environment. Mice were anaesthetized and mounted on a custom-built stage connected to a suck ring pump device to visualize the liver microcirculation.

II.2.14. Cell culture

Cell culture allows maintenance and growth of cells in an artificial environment. In this study the following cell lines were used: L3.6pl cell line, human pancreatic cancer cell line and KPC cell line, a mouse pancreatic cancer cell line which was isolated from genetically modified mice (*LSL-$Kras^{G12D/+}$; LSL-$Trp53^{R172H/+}$; Pdx-1-Cre)*. L3.6pl and KPC cell lines were cultured in high glucose DMEM medium (4.5 g/l) with 2.5% NEAA, 10% FBS and 1% pen/ strep and low glucose DMEM (1g/l) with 10% FBS, 2.5% NEAA, 2.5% vitamins and 1% pen-strep, respectively. All the cells were grown in cell culture flasks of various sizes as per requirement and maintained in an incubator with relative humidity, CO_2; 5%, at a temperature of 37°C.

II.2.15. Isolation of MVs

For MV isolation from L3.6pl and KPC cells, both cell cultures were suspended from the petri dishes in low glucose DMEM (1g/l) with low FBS (2%) followed by collection of the supernatants. Afterwards supernatants were subjected to initial centrifugation at 1,300 rpm for 10 min without break to remove large cells. The pellet was discarded and the supernatant was then centrifuged at 1,430 g for 20 min to get rid of large vesicles, cell debris and platelets. After centrifugation the supernatant was collected and again centrifuged (1,430 g for 20 min). The supernatant was

recovered and centrifuged at 17,750 g for 30 min. Supernatant was discarded and the pellet containing the MVs was resuspended and centrifuged at 17,750 g for 30 min. The pellet was recovered and resuspended in appropriate medium for further analysis.

II.2.16. Protein estimation

The amount of protein present was determined immediately after the end of experiment using an end point chromogenic assay (Bradford's assay). Samples were resuspended in a minimum volume of 500 µl PBS. Serial dilutions ranging from 2 mg/ml to 0.03906 mg/ml were made using a standard protein solution of 2 mg/ml BSA. 5 µl of the standards and samples were added in triplicates to 96-well plates. 25 µl of copper-alkali-tartrate solution A, which forms a complex with the proteins in the suspension, was added to each well. Then, 200 µl of solution B, which reduces the protein complex to generate blue color was added to each of the wells above. The absorbance was measured at 700 nm and protein concentration of the samples was calculated form the standard curve using excel scatter graph format.

II.2.17. Electron microscopy

To check the purity and quality of the MV preparations, the vesicle suspensions were fixed for 1 hr. Fixation was performed using 2.5 % glutaraldehyde in 75 mM cacodylate buffer also containing 2 mM $MgCl_2$ and 2 mM NaCl. After fixation the samples were processed for transmission electron microscopy (TEM) and scanning electron microscopy (SEM). For TEM, 5 µl of the sample was applied to carbon-coated copper grids and negatively-stained with 2% uranyl acetate. For SEM, the fixed samples were frozen to glass slides with liquid nitrogen, washed 4 times with buffer (5, 10, 30, 60 min), post-fixed with 1% aqueous osmium tetroxide for 1 h, washed again twice with buffer (10 min, overnight) and 3 times with double distilled water (5, 20, 30 min). After dehydration with a graded acetone series, the samples were critical-point-dried. The glass slides were mounted onto aluminum stubs and sputter-coated with platinum for 40 s. TEM was carried out on a Zeiss EM 912 at 80 kV. Images were acquired using a Tröndle 2k x 2k slow-scan CCD camera. For SEM, a Hitachi S-4100 SEM was used with the acceleration voltage set to 3 kV.

II.2.18. Nanoparticle tracking analysis

The isolated MVs were resuspended in PBS and applied to a ZetaView PMX 110 instrument by using a syringe. Different dilutions were made from each sample and all the samples were measured

at 11 different positions. Three cycles of reading were performed for each position. Polystyrol beads of known concentration and diameter (100 nm) were used for calibration. Post-acquisition parameters were set to a minimum brightness of 5, a resolution of 100 pixels and 30 frames/s.

II.2.19. Animal experiments

MVs (100 µg) protein were labelled with DiD and injected into the tail vein of WT mice (9- 12 weeks). In some cases the animals were pre-treated with anti-CD36 antibody (3 mg/kg body weight) before injecting MVs. The injection scheme for the animal experiments was performed as described in scheme below:

0----------1h ----------2h
Anti-CD 36 ----------MV/ PBS (100 µg) --------- sacrifice and organ collection.

Long-term experiments were also performed, where the animals were sacrificed after 4 day, 8 days or 14 days after the MV and/ or cancer cell injections.

0----------10min----------1h----------Day 4 / Day 8/ Day 14
MV/ PBS (75 µg) + MV/ PBS (75 µg) --- Cancer cell inject---------- sacrifice and organ collection.

During long-term experiments (up to 14 days) anti-CD36 antibody (3 mg/kg body weight) was infused every second day.

II.2.20. Super-resolution microscopy

Stimulated emission depletion (STED) nanoscopic imaging was used to double label the tumor MVs. SYTO RNASelect (500 nM, 20 min; Thermo Fisher Scientific), pHrodo (5 µM, 30 min; Thermo Fisher Scientific), DiD or Vybrant DiL were used to label the membrane and the intravesicular cargo of the MVs. Human monocytic THP-1-cells were cultured in RPMI1640 medium with 10 mM hepes (Merck) and 10% heat-inactivated FBS and were stimulated with PMA (300 nM, Merck) overnight to differentiate them into macrophages. Macrophages were then labelled with FM-464FX and incubated with double labeled tumor MVs for 60 min. After 60 min the cells were fixed with 2% PFA at 4°C for 15 min. Mounting was done using mowiol or Prolong Diamond Antifade Mountant (Thermo Fisher Scientific). The samples were analyzed using a Leica SP8 STED 3X (Leica, Germany). Images were reconstructed by using the LAS X software package (version 3.0; Leica, Germany) and deconvolution (CMLE algorithm) was introduced by using

Huygens Professional software package (version 16.10; Scientific Volume Imaging, the Netherlands).

II.2.21. Statistics

All mean values are given ± s.e.m. P values < 0.05 were considered to be significant. The results were compared by two-tailed unpaired *t*-test using Bonferroni corrections and Mann-Whitney rank-sum test for multiple comparisons or one way ANOVA or two way ANNOVA. All-values given refer to different experiments or different animals.

III. Results

III.1. Microvascular fibrin generation during systemic bacterial infection

III.1.1. Infection kinetics and microvascular coagulation analysis in WT mice

C57BL/6J mice were injected with 3.2 x 10^8 *E.coli* via the tail vein for the different time intervals (1 hr, 3 hr and 6 hr). To analyze the infection kinetics, CFUs were measured in the liver, spleen, kidney, lung, heart and the brain.

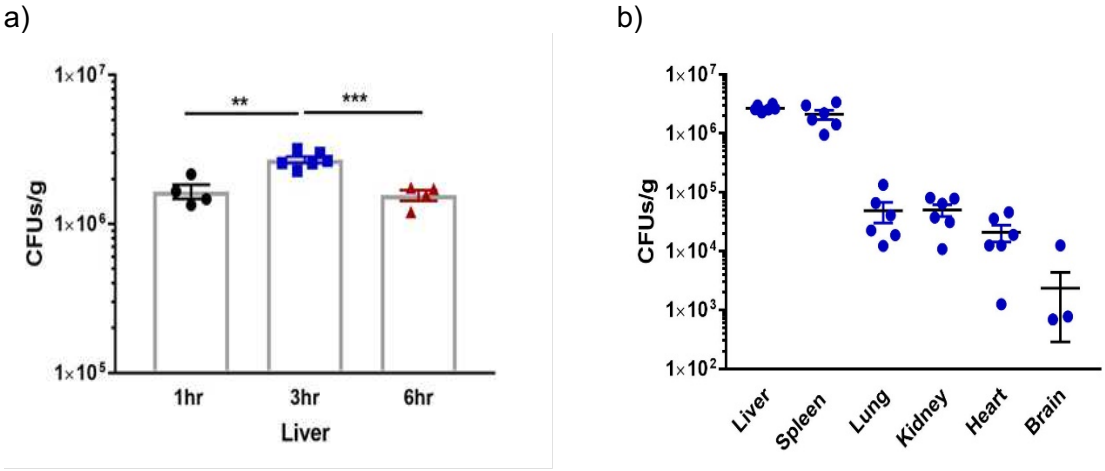

Figure 8: Kinetics of systemic infection with *E.coli*. a) CFU analysis in the *E.coli* infected liver after 1 hr, 3 hr and 6 hr. b) CFU measurements in the liver, spleen, lung, heart and the brain at 3 hr post infection. n = 3-6; animal number per group. Mean +/- SEM. ** p <0.01, *** p <0.001.

Fig. 8a shows a peak of infection in the liver occurred at 3 hr post infection. The liver and the spleen harboured the greatest amount of bacteria when compared to other organs (Fig. 8b). This altogether confirms the role of the liver and the spleen as organs of immune tolerance and suggests that the resolution of the intravascular circulating *E.coli* starts potentially at 6 hr post infection.

As a next step, to check for the localization of the bacteria in the liver microcirculation, we performed immunostaining of liver cryosections. Liver sinusoids were stained with anti-stabilin2 antibody (orange), fibrin was visualized by using anti-fibrin antibody (red) and bacteria that genetically expressed the GFP (Fig 9a, b).

Fibrin was quantified using the ZEN program by determining the total vessel area, as well as the area covered by fibrin inside the vessel. The analysed images showed that bacteria was entrapped by the fibrin in the microvasculature (Fig 9a). As shown in Fig. 9b, a method was developed and later being used for analysing the percentage of fibrin inside liver sinusoids.

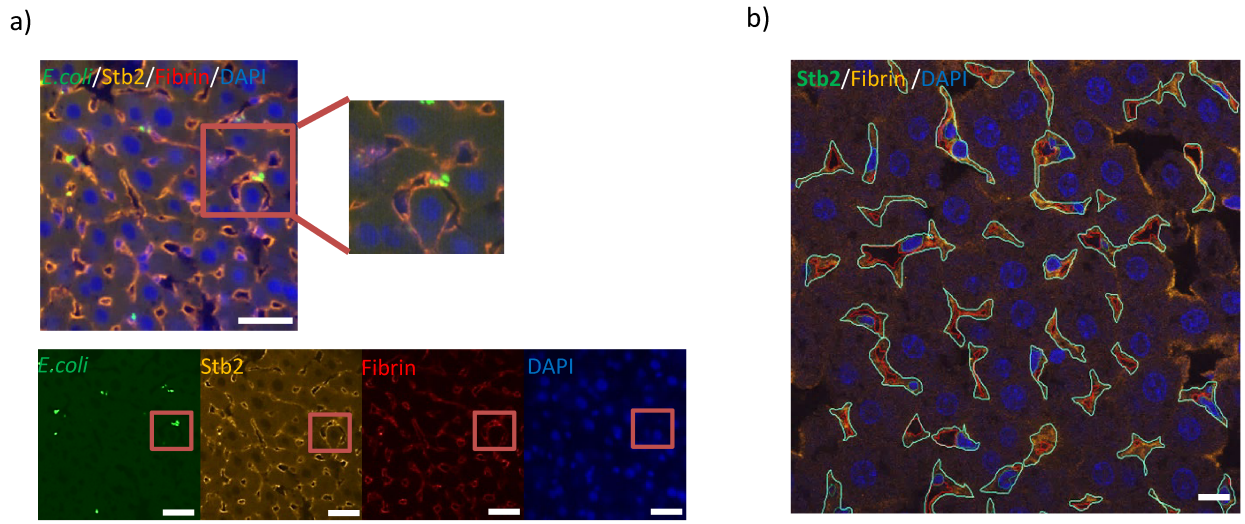

Figure 9: a) Qualitative analysis of bacterial localization in the liver vasculature. GFP labelled *E.coli*, (Green). Anti-stabilin 2 antibody, (Orange). Anti-fibrin antibody (Red). Scale bars: 20 µm. b) Total intravascular area of microvessels and fibrin covered area in liver cryo- section 3 hr after infection. Scale bars: 10 µm.

To investigate the correlation between the coagulation and the infection, the fibrin formation was analysed at different time points (Fig. 10).

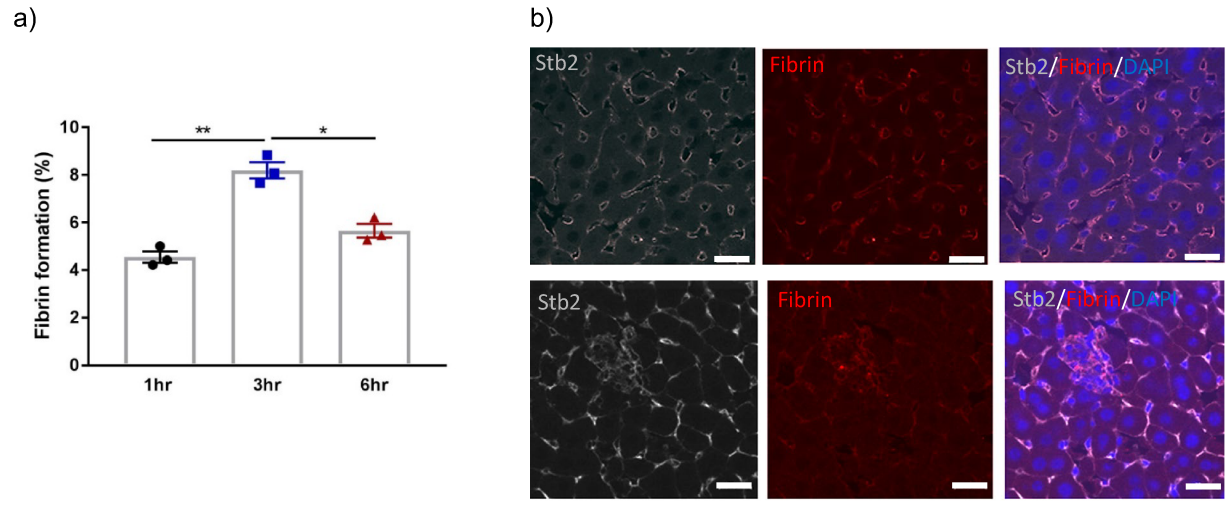

Figure 10: a) Quantitative measure of fibrin formation (%) in the liver microcirculation during *E.coli* infection at various time points. b) Representative images of fibrin formation at 3 hr (upper panel) and 6 hr (lower panel). Pseudo coloured grey; Alexa 546- secondary antibody (stabilin2). Red; Alexa 594-secondary antibody (fibrin), DAPI (blue). Scale bars: 20 µm. n = 3; animal number per group. Mean +/- SEM. *p< 0.05, ** p <0.01.

Fibrin analyses show a peak of microvascular coagulation at the 3 hr time point (Fig. 10a and b) which suggests a possible correlation of a high bacterial number (Fig. 8a) with a high fibrin formation at 3 hr post infection.

III.1.2. Infection kinetics and microvascular coagulation in gene-edited mice models

III.1.2.1. Role of MIF during systemic bacterial infection

To search for cytokine mediators of immunothrombosis we investigated the function of MIF, a pro-inflammatory cytokine during systemic infection. The infection kinetics as well as fibrin formation were performed in mice deficient for MIF (MIF-/- mice).

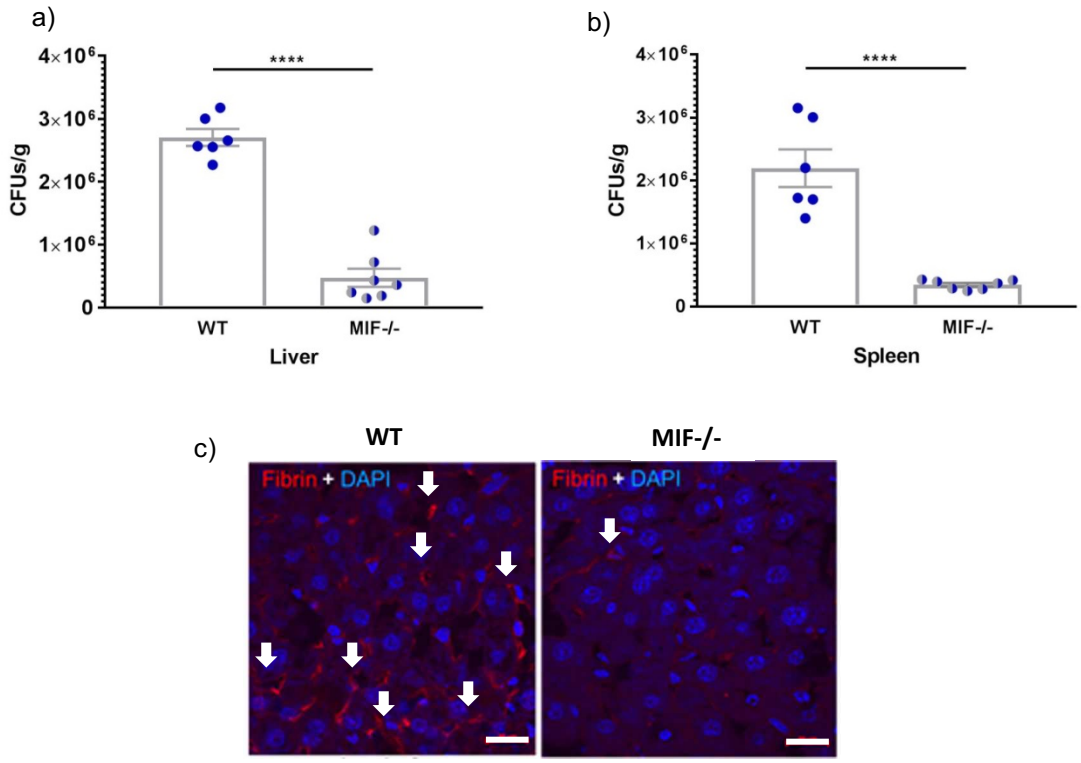

Figure 11: a) CFU measurements in the liver 3 hr after infection in WT and MIF-/- mice. b) CFU measurements in the spleen 3 hr after infection in WT and MIF-/- mice. C) Confocal images of fibrin formation in the liver of WT (left) and MIF-/- (right) mice at 3 hr post infection. Arrows represent fibrin-rich areas inside the microvessels. Scale bars: 20 µm. n = 5; animal number per group. Mean +/- SEM. ****p< 0.0001

Fig. 11a and b indicate very strong effects of MIF on bacterial survival as the CFUs were massively reduced in both the liver and the spleen of MIF-/- mice when compared to WT mice. Fibrin

formation was also influenced by MIF as the coagulation activation was clearly lowered in mice lacking MIF (Fig. 11c).

III.1.2.2. Role of uPAR and PLG during systemic bacterial infection

To reveal how the fibrinolytic system affects the systemic bacterial infection, *E.coli* was injected into uPAR-/- and PLG-/- mice. CFU analyses were done in the liver and spleen (Fig. 12a, b).

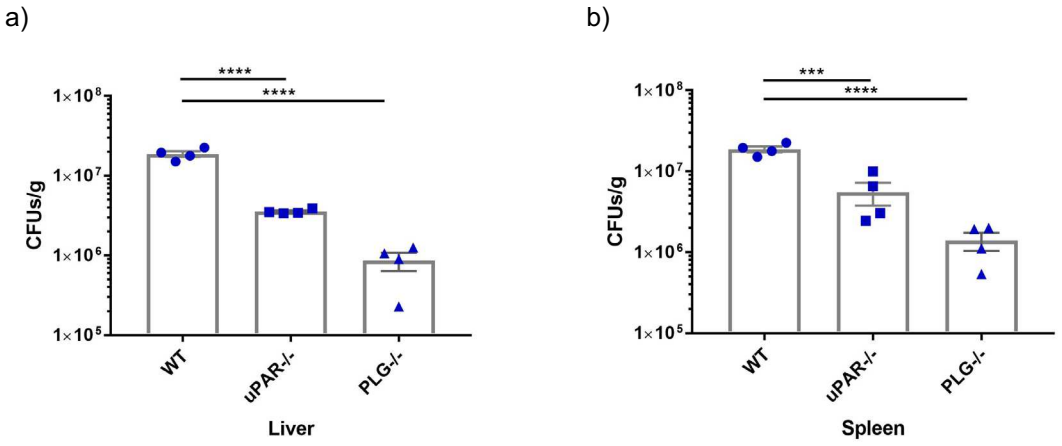

Figure 12: a) CFU measurements in the liver 3 hr after infection in WT, uPAR-/- and PLG-/- mice. b) CFU measurements in the spleen 3 hr after infection in WT control, uPAR-/- and PLG-/- mice. n = 4; animal number per group. Mean +/- SEM. ***p< 0.001, ****p< 0.0001

Fig. 12a, b indicates the effect of uPAR and PLG on bacterial growth in both the liver and spleen. Bacterial survival is massively decreased at 3 hr when compared to WT animals. At the same time, representative pictures for fibrin formation (Fig. 13) show a marked increase of coagulation in uPAR-/- and PLG-/- mice.

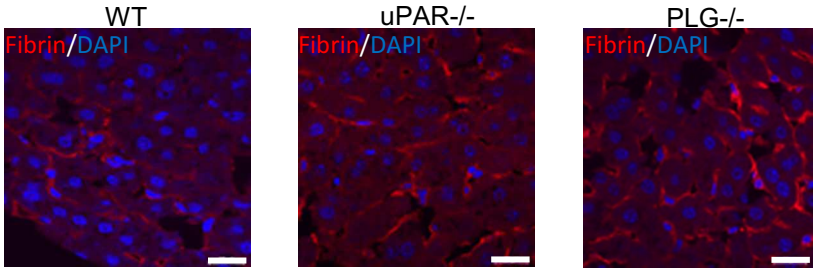

Figure 13: Representative images of fibrin formation in WT (left), uPAR-/- (middle) and PLG-/- (right) mice at 3 hr. Scale bars: 20 µm. n = 4; animal number per group.

To check the effects of fibrinolysis at later time points, the experiments were also performed at 18 hr after infection. CFUs were measured in the liver and the spleen (Fig. 14a, b).

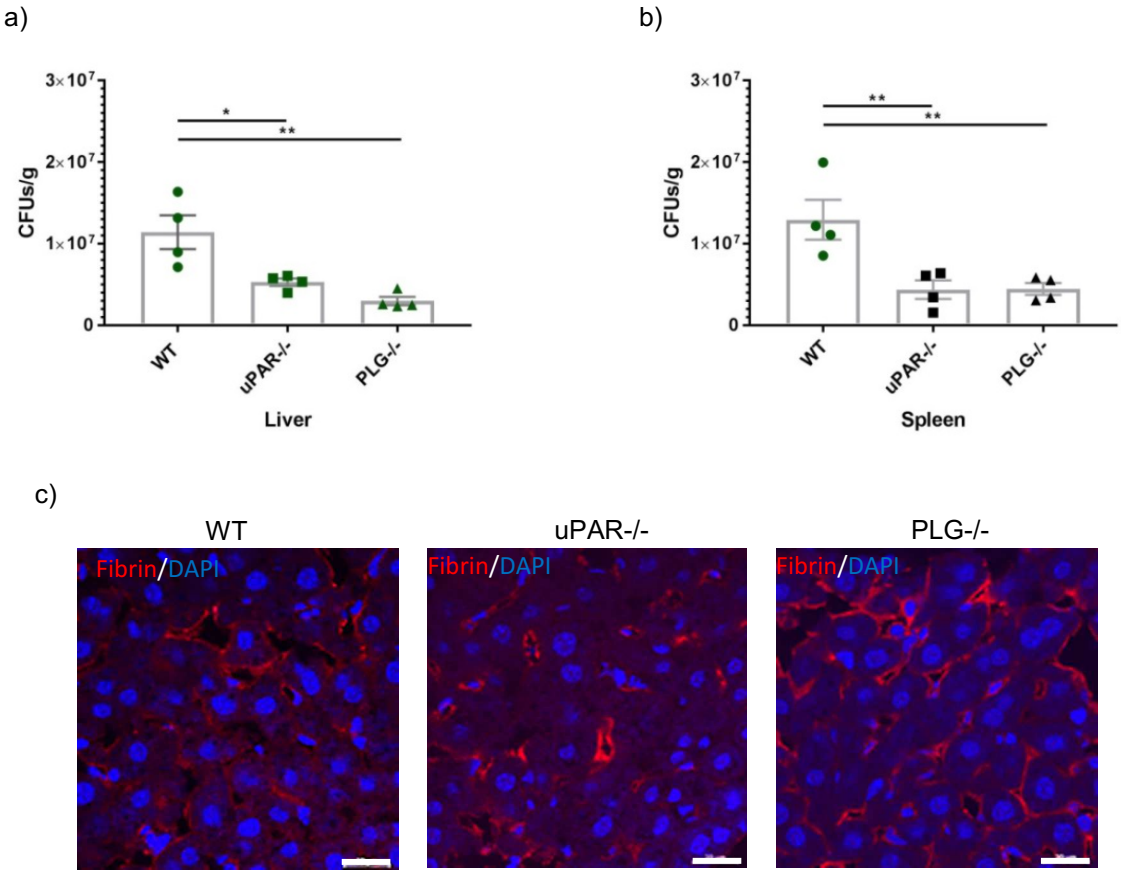

Figure 14: a) CFU measurements in the liver 18 hr after *E.coli* infection in WT control, uPAR-/- and PLG-/- mice. b) CFU measurements in the spleen 18 hr after *E.coli* infection in WT control, uPAR-/- and PLG-/- mice. c) Representative pictures of fibrin formation in WT (left), uPAR-/- (middle) and PLG-/- (right) at 18 hr. Scale bars: 20 µm. n = 4; animal number per group. Mean +/- SEM. *p< 0.05, ** p <0.01.

Although less prominent, inhibition of fibrinolysis also increased bacterial elimination at 18 hr. Fig. 14 c shows an increased fibrin formation in uPAR-/- and PLG-/- as compared to WT mice at the 18 hr time point.

Both after 3 hr and 18 hr also quantitative measurements of fibrin positive microvessels were performed (Fig. 15a, b). The fibrin formation data (Fig. 15a) from WT, uPAR-/- and PLG -/- mice point towards the importance of fibrin in bacterial clearance since increased fibrin formation was associated with a reduced bacterial survival.

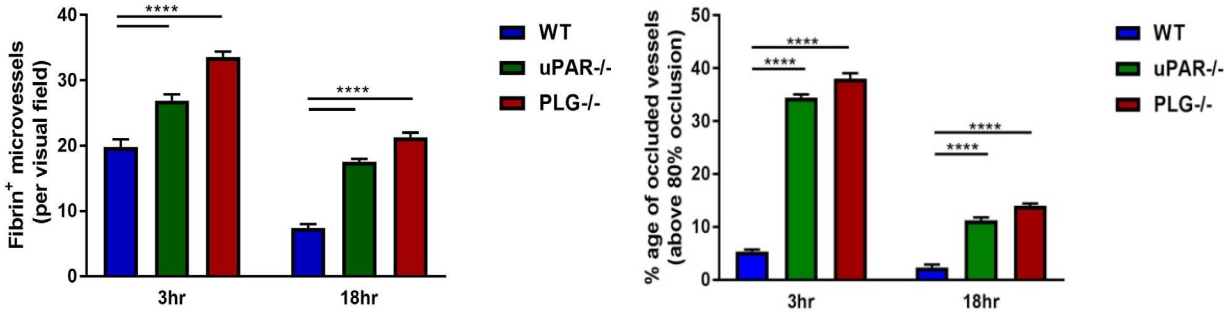

Figure 15: a) Fibrin positive microvessels at 3 hr and 18 hr post infection in WT control, uPAR-/- and PLG-/- mice. b) Percentage of occluded vessels (above 80%) at 3 hr and 18 hr post infection in WT control, uPAR-/- and PLG-/- mice. n = 4; animal number per group. Mean +/- SEM. **** $p < 0.0001$.

Moreover, the increased occlusions of liver microvessels in uPAR-/- and PLG-/- mice compared to WT mice emphasize the role of fibrinolysis in maintaining blood perfusion in the microcirculation during systemic infection.

III.2. Immune cell recruitment to the microcirculation during *E.coli* infection

To identify the immune cells recruited to the liver microvasculature at various stages of intravascular coagulation (Fig. 16a) we analyzed accretion of all nucleated cells and platelets to the liver microcirculation. Moreover, it was analyzed whether these immune cells expressed or bound fibrinolytic proteins and endogenous anticoagulation proteins.

Fig. 16a shows that platelets recruitment peaked at 1 hr, T cells and neutrophils at 6 hr and C monocytes at 3 hr. recruitment of platelets, neutrophils, C monocytes, NC monocytes and B cells are shown in Fig. 16b.

a)

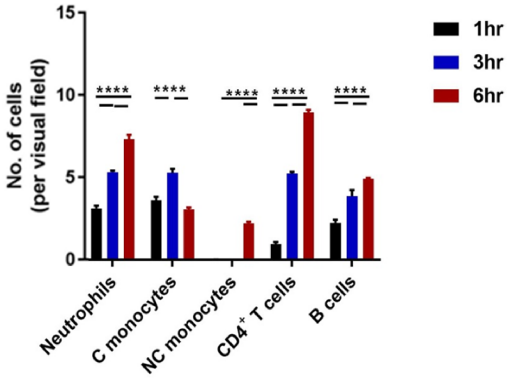

b)

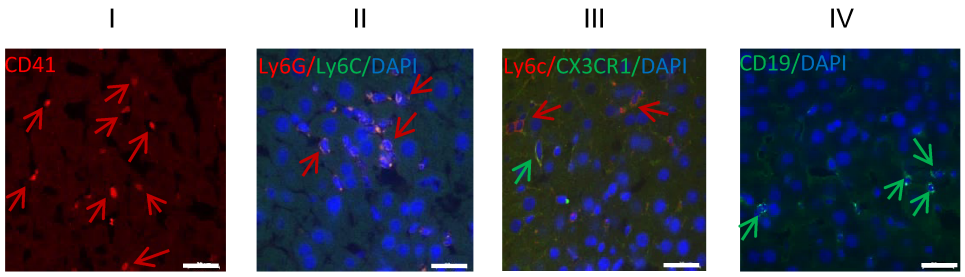

Figure 16: a) Immune cell recruitment to the liver microvasculature at various time points in *E.coli* infected WT mice. b) Representative images of platelets (I) at 1 hr, neutrophils clusters (II) at 6 hr, NC monocytes (green arrows). (III) at 6 hr and B cells (green arrows) (IV) at 6 hr. Scale bars: 20 µm. n = 3-4; animal number per group. Mean +/- SEM. **** p <0.0001.

Immune cell recruitment was also analysed in uPAR-/- and PLG-/- mice as compared to WT mice at 3 hr post infection (Fig. 17).

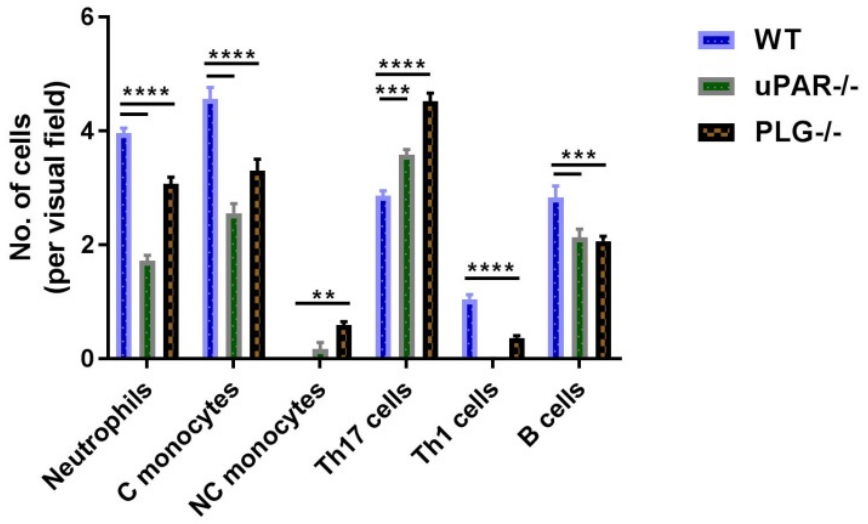

Figure 17: Immune cell recruitment to liver microvasculature at 3 hr post infection in WT control, uPAR-/- and PLG-/- mice. n = 3-4; animal number per group. Mean +/- SEM. **p<0.01, ***p< 0.001, **** p <0.0001.

In uPAR-/- and PLG-/- the influx of immune cells into the liver microvasculature was clearly changed (Fig. 17). The recruitment of neutrophils, C monocytes, Th1 cells and B cells was reduced, while the accretion of NC monocytes and Th17 was enhances in the liver microcirculation.

III.3. Fibrinolytic proteins

Proteins like tPA or uPA are key players of fibrinolysis as they activate plasminogen to plasmin which further leads to degradation of fibrin. To visualize the time dependence of the cellular binding of uPA and its receptor uPAR in the liver microcirculation of infected mice, immunostaining was performed to detect cells positive for fibrinolytic proteins (Fig. 18a, b).

Fig. 18a, b and c show a gradual increase of uPA and uPAR positive cells between 1 hr and 6 hr. A peak was revealed at 6 hr after infection.

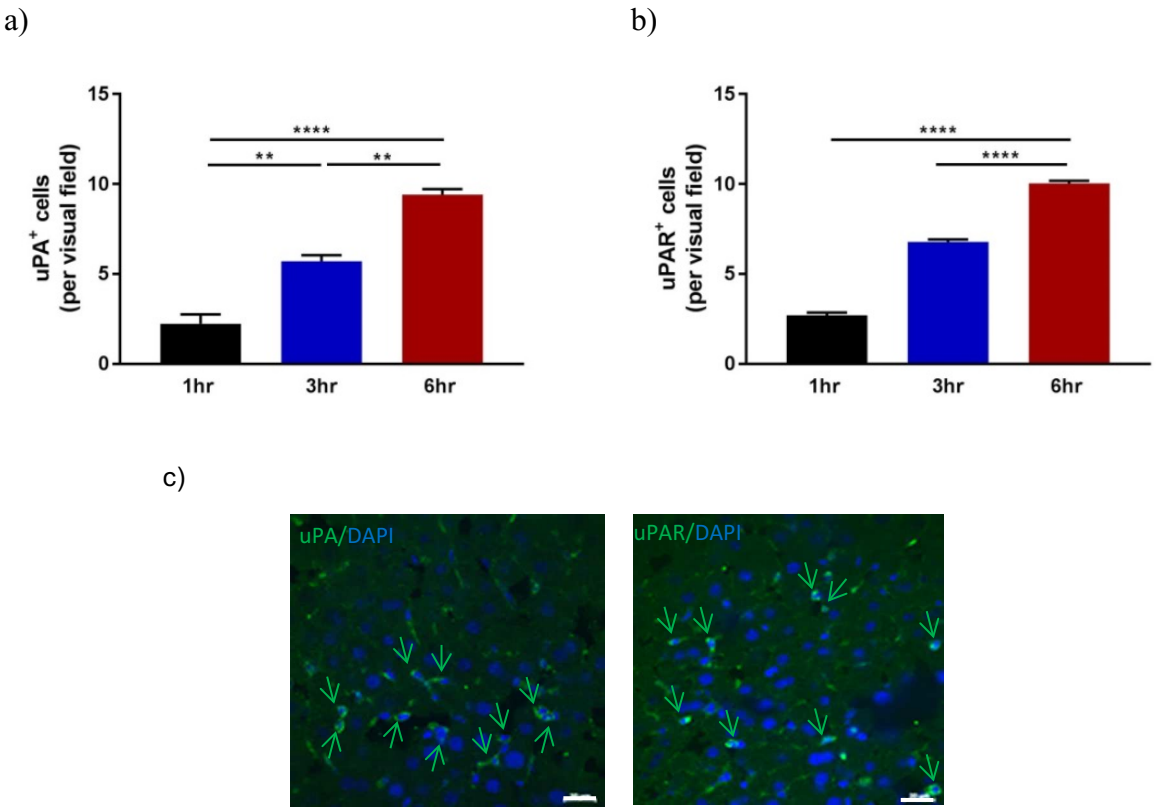

Figure 18: Time dependence of (a) uPA and (b) uPAR- positive cells at 1 hr, 3 hr and 6 hr after infection in WT mice. c) Representative pictures of uPA and uPAR positive cells at 6 hr. Scale bars: 20 µm. n = 3-4; animal number per group. Mean +/- SEM. **p<0.01, **** p <0.0001.

Furthermore, in comparable experiments the number of tPA positive cells were assessed (Fig. 19a). In addition cells positive for PAI-1 were imaged (Fig. 19b), which is a strong inhibitor of fibrinolysis.

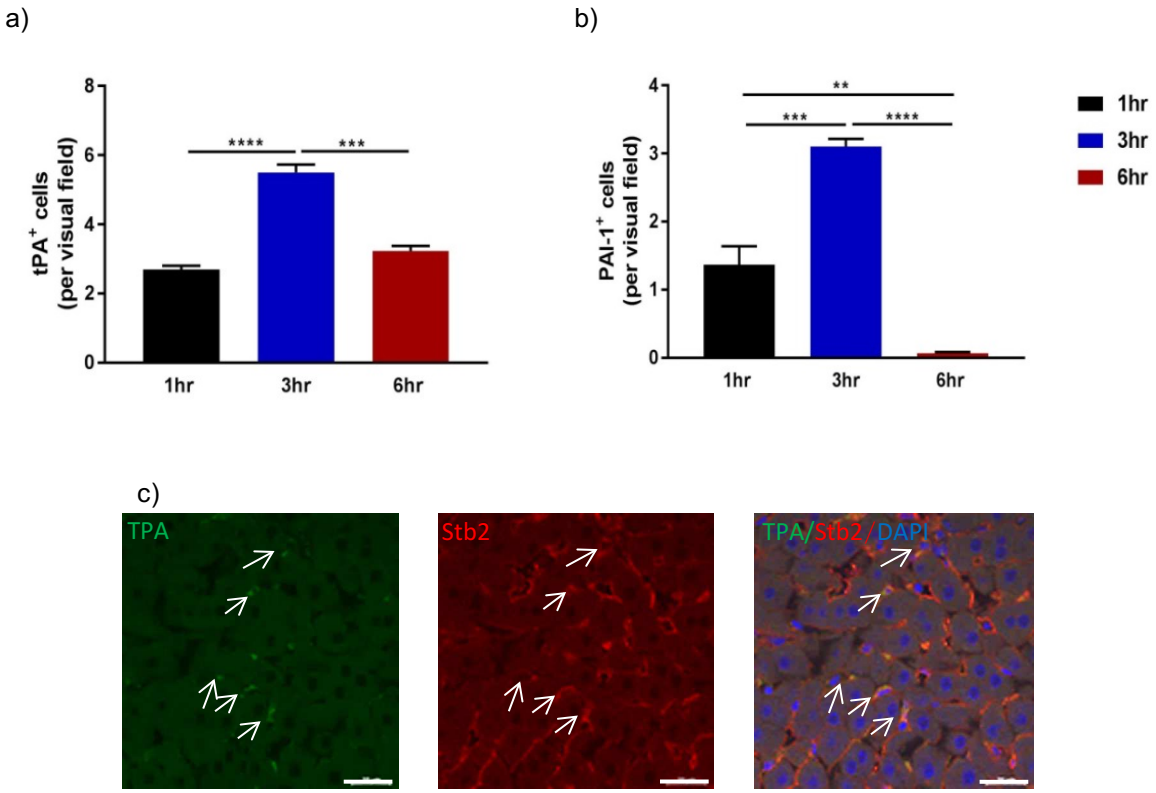

Figure 19: Time dependence of a) tPA and b) PAI-1 positive cells at 1 hr, 3 hr and 6 hr after infection in the liver microcirculation of WT mice. c) Representative pictures of tPA positive cells at 3 hr. Scale bars: 20 µm. n = 3-4; animal number per group. Mean +/- SEM. **p<0.01, ***p< 0.001, **** p <0.0001.

Fig. 19a and c shows the time dependence of appearance of tPA positive cells. A peak is observed at 3 hr after infection. A peak of the appearance of PAI-1 positive cells is also observed after 3 hr (Fig. 19b). Thereafter PAI-1 disappear completely which coincides with the fall in fibrin formation after 6 hr (Fig.10a).

III.4. Colocalization of distinct immune cells with fibrinolytic proteins

To identify immune cells potentially involved in fibrinolysis during systemic bacterial infection, immunofluorescence staining was performed and colocalization of neutrophils, C monocytes, NC monocytes and $CD4^+$ T cells with uPA (Fig. 20a) and uPAR (Fig. 20b) was analyzed at different time points.

a) b)

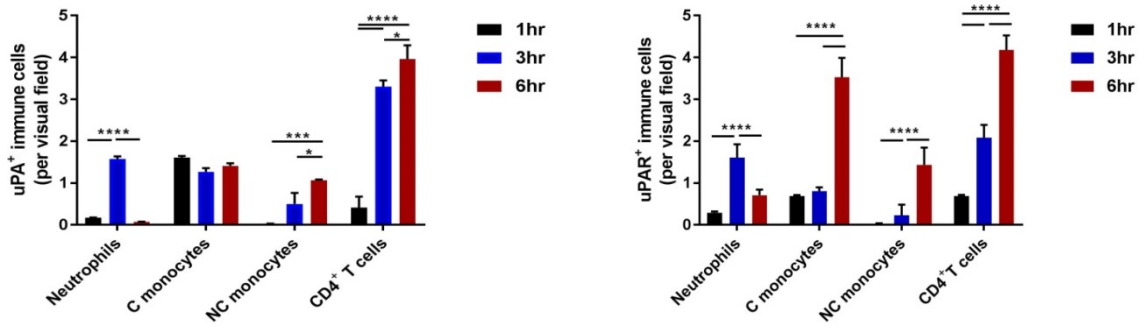

Figure 20: Colocalization of recruited immune cells with a) uPA and b) uPAR at 1 hr, 3 hr and 6 hr after infection in WT mice. n = 3-4; animal number per group. Mean +/- SEM. *p<0.05, ***p<0.001, **** p <0.0001.

Fig. 20 a, and b show that colocalization of neutrophils with uPA and uPAR is maximal at 3 hr. At 6 hr, NC monocytes and $CD4^+$ T cells substantially colocalize with uPA and uPAR. C monocytes express uPAR receptor on their surface in particular at 6 hr. The strongest colocalization of uPA and uPAR with immune cells is seen with $CD4^+$ T cells at 6 hr (Fig. 20a, b).

III.5. $CD4^+$ T cells during systemic bacterial infection

III.5.1. Depletion experiments

Given that $CD4^+$ T cells were present in massive numbers at earlier time points (Fig. 16a) and strongly colocalized with uPA and uPAR (Fig. 20a, b) , the next step was to analyze their role in systemic bacterial infection. To this purpose Iso-IgG antibody or neutralizing anti-CD4 antibody (100 µg) was infused 24 hr prior to *E.coli* supplementation (scheme D, section: II.2.2.).

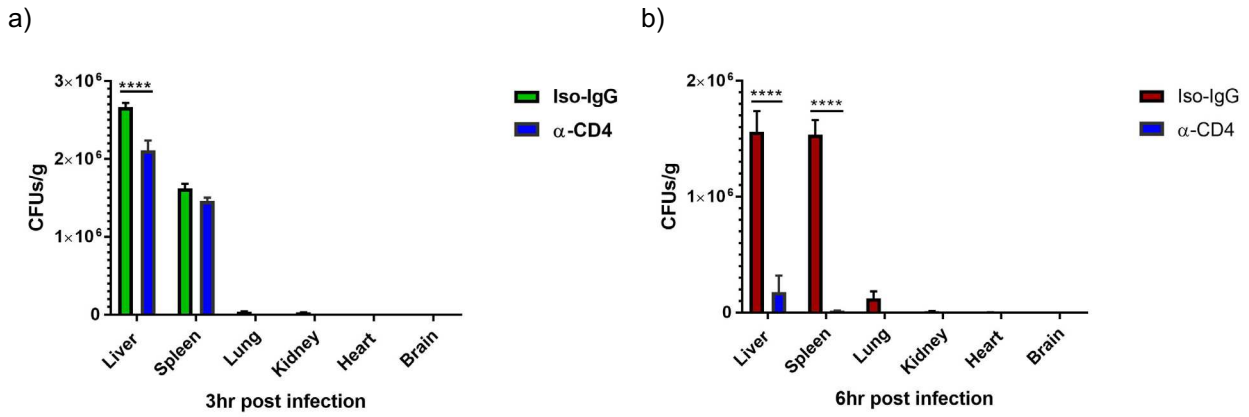

Figure 21: CFU measurements in Iso-IgG control injected mice and CD4 neutralizing ab injected mice at a) 3 hr and b) 6 hr after infection. n = 3-4; animal number per group. Mean +/- SEM. **** p <0.0001.

After 3 hr and 6 hr post infection we assessed CFUs in major organs. CFUs were reduced in the liver of CD4-depleted animals compared to Iso-IgG injected mice both at 3 hr (Fig. 21a) and more profoundly at 6 hr (Fig. 21b). At 6 hr also splenic CFUs were diminished. Increased formation of fibrin was also analyzed in CD4-depleted animals as compared to the Iso-IgG control (data not shown). Furthermore, to identify the subtypes of $CD4^+$ T cell recruited at 3 hr post infection; we performed staining with various antibodies. As a result, most of the $CD4^+$ T cells were found to represent Th17 cells (Fig. 22).

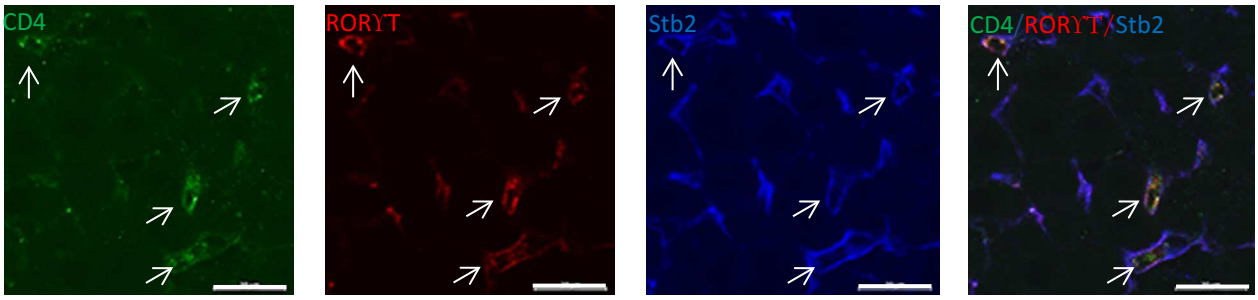

Figure 22: Identification of $CD4^+$T cell subtype as Th17 cells in liver microvessels at 3 hr post infection (anti-CD4 ab-488, anti-RORγt ab; secondary ab alexa fluor 594, anti-stb2 ab; secondary ab alexa fluor 550; pseudocolor in blue). Scale bar: 20 µm.

III.5.2. Recruitment of Th17 cells

To investigate how Th17 cells are recruited to the site of bacterial adhesion and to track the Th17 cell mobilization from one organ to other organ, we have applied the photoactivation method to Kaede mice. Kaede mice expressing Th17 (green) were photoconverted by using a UV light exposition in the small intestine (their major site of localization) and the Th 17 converted cells (red) were quantified in the liver and lung after 6hr of infection.

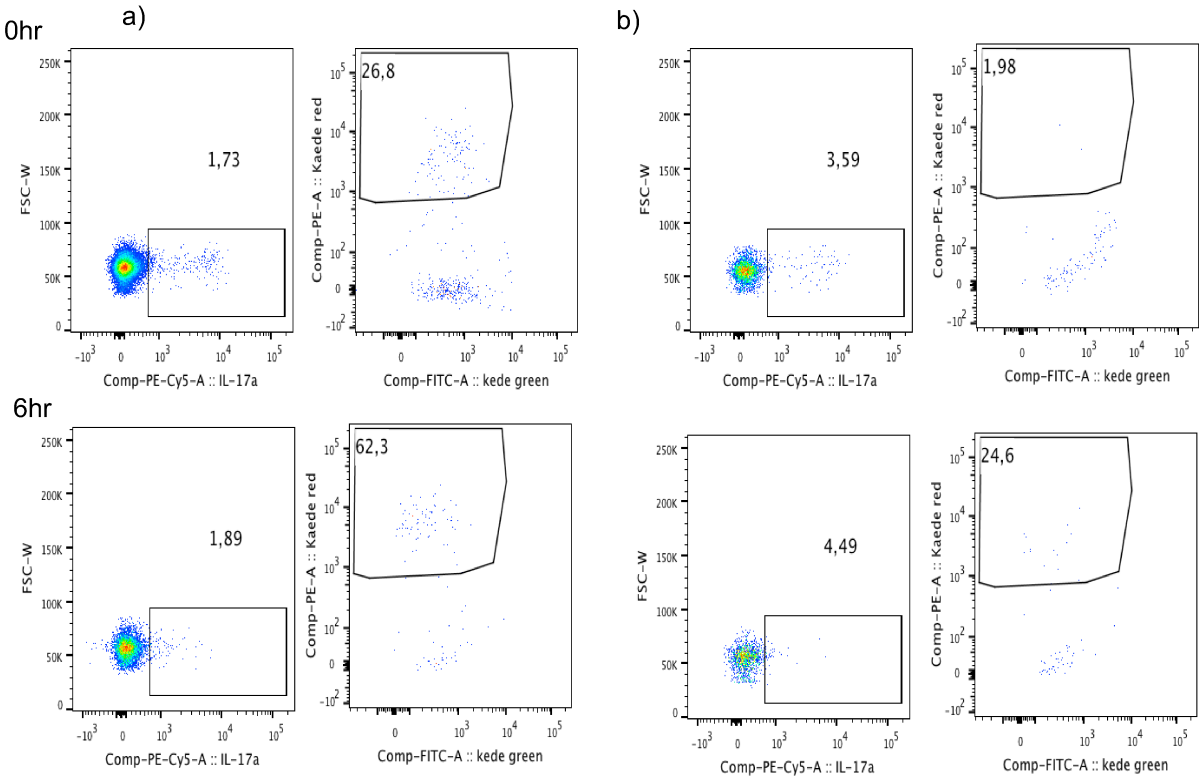

Figure 23: Flow cytometry analysis of Kaede photo-converted IL-17a positive Th17 cells mice. a) FACS photoconvertion in the liver and b) the lung at 0 hr and 6 hr.

After the selective exposure of the small intestine for 60 s, Kaede –photo-conversion was specific to small intestine. 24 hr later *E.coli* was injected via the tail vein followed by sacrificing the mice after 3 hr and 6 hr. The percentage of Kaede red photo-converted cells was measured in the liver at 3 hr and 6 hr post infection via FACS (Fig. 23). Two types of control groups were analyzed in parallel: photoconverted control mice and non-infected mice.

The percentage of IL-17A- positive photoconverted cells was significantly higher in the liver after 6 hr of infection compared to the control at 0 hr (Fig. 24). These findings suggested that part of

Th17 cells recruited to adherent bacteria in the liver microcirculation during infection is derived from the small intestine (Fig. 24).

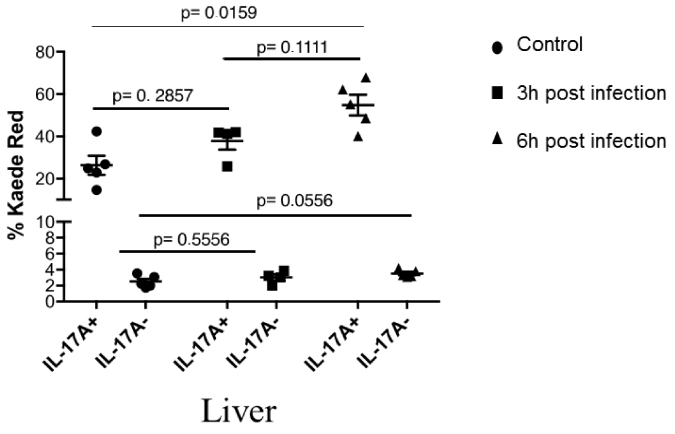

Figure 24: Percentage of Kaede red photo-converted cells in the liver and n = 3-4; animal number per group. Mean +/- SEM.

III.5.3. Colocalization of Th17 cells with fibrinolytic and pro-coagulant proteins

Next, we tested the potential colocalization of Th17 cells with uPA and TF, the fibrinolytic and procoagulant proteins respectively. Immunofluorescence was performed in *E.coli* infected livers using markers for Th17 (CD4 and RORγT) and for fibrinolytic proteins uPA (Fig. 25). The measurements were performed 6 hr because this time point positively for fibrinolytic proteins was highest.

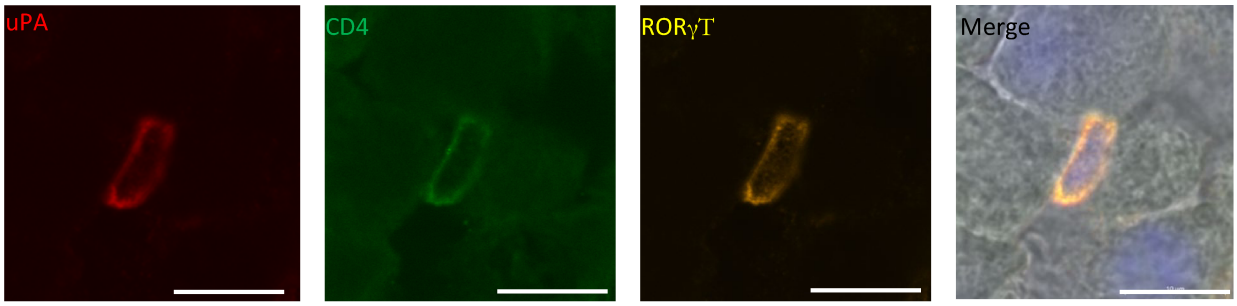

Figure 25: uPA positive Th17 cell at 6 hr post infection. anti-CD4 antibody (green), anti-RORγt antibody (orange), anti-uPA antibody (red). Scale bar: 10 µm.

We also checked TF expression on Th17 cells at 1 hr after infection since TF positivity was higher at this point (Fig. 26). TF was detected on the surface of the Th17 cells. Together these findings suggest a plasticity in the role of Th17 during various stages of infection.

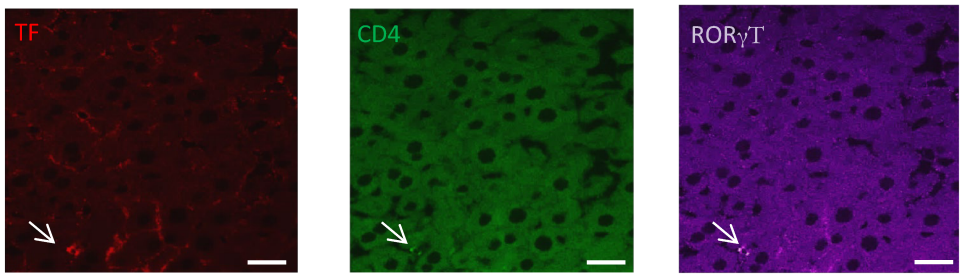

Figure 26: TF colocalization with Th17 cell at 1 hr post infection. (1H1- antibody (red), anti-CD4 antibody (green), anti RORγt antibody (pseudocolored- violet). Scale bar: 20 µm.

III.5.4. Plasmin formation assay with isolated Th17 cells in vitro

Since uPA was colocalized with Th17 cells *in vivo* (Fig. 25) we next analyzed whether Th17 cells had pro-fibrinolytic activity *ex vivo* (Fig. 27). Naïve T cells were isolated from the lymph nodes of *E.coli* infected mice. Then a cytokine cocktail was added to differentiate them into two different phenotypes; anti-inflammatory and pro-inflammatory. The *in vitro* assays were performed using pre formed clots to determine the fibrinolytic activity of Th17 cell subtypes.

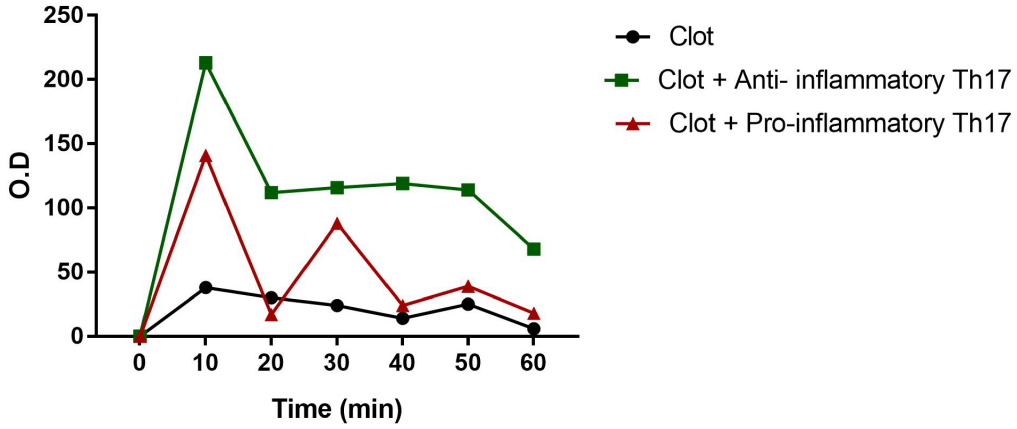

Figure 27: Fibrinolytic activity of subtypes of different Th17 cells *in vitro*. Representative experiment of 3 different experiments.

Fig. 27 shows that the anti-inflammatory subtype of Th17 cells supported the highest fibrinolytic, whereas the pro-inflammatory subtype had a lower fibrinolytic activity.

III.5.5. Il23R-/- mice experiments

To analyze the role of Th17 cells for the outcome of the systemic infection we performed some experiments with IL23R-/- mice. CFUs were measured in *E.coli* injected IL23R-/- mice and WT mice after 6 hr of infection (Fig. 28).

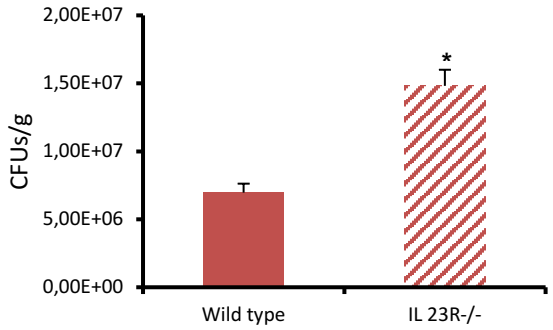

Figure 28: Bacterial survival in the liver of WT and IL23R-/- mice 6 hr after infection. n = 3-4; animal number per group. Mean +/- SEM. * p <0.05.

FACS analyses of the livers of IL23R-GFP mice indicated that in these animals apart from Th17 cells also γδ T cells, NKT cells and innate lymphoid cells were labelled (data not shown). Moreover, analyses of FACS data (not shown) suggested that most of the cells that were IL23R-GFP positive were γδ T cells. Therefore, IL23R-/- mouse model was not further analyzed. However, Fig. 28 shows that IL23R positive cells are involved in bacterial killing.

III.6. Role of NC monocytes during the resolution of systemic bacterial infection

III.6.1. NC monocyte recruitment

Long-term infection experiments were performed by using smaller amount of bacteria (5 x 10^7) in mice infected for 6 hr, 24 hr and 48 hr with *E.coli*. NC monocytes were detected in the liver microcirculation using anti-CX3CR1 antibody, anti-Ly6C antibody and anti-stabilin 2 as a marker for the microvessels.

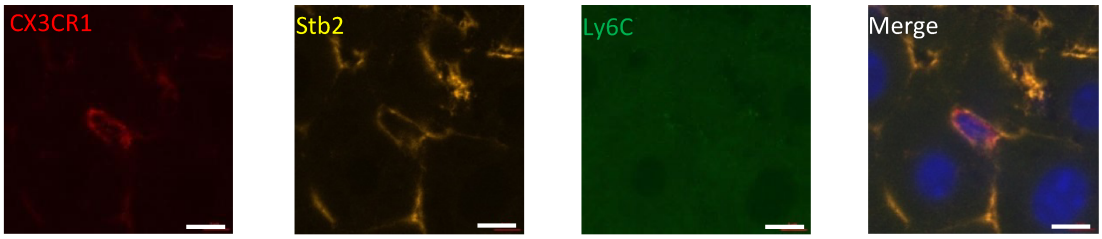

Figure 29: Identification of NC monocytes by expression analyses of $CX3CR1^+$ (red) stab2 (orange) Ly6C (green) cells in liver microvessels 6 hr post infection. Scale bar: 5 µm.

The intravascular cells that were positive for CX3CR1 but negatively stained for Ly6C were considered as NC monocytes present in microcirculatory vessels (Fig. 29). Next, quantitative analyses of the recruited NC monocytes indicated their arrival at 6 hr that was followed by a strong increase at 24 hr and 48 hr (Fig. 30).

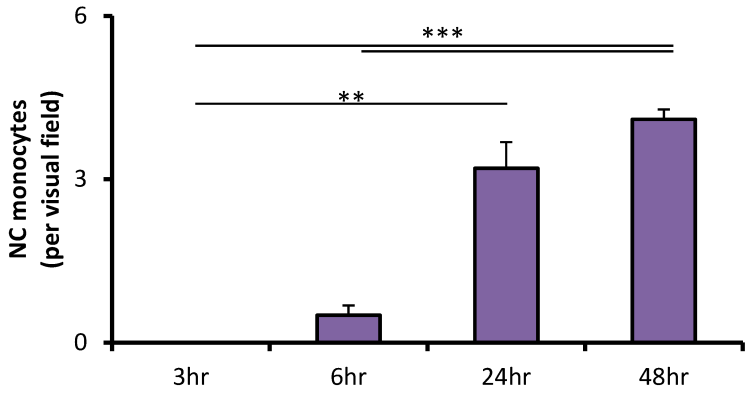

Figure 30: Quantitative analysis of recruitment of NC monocytes to the liver microcirculation in mice infected with *E.coli* (5x10^7). n = 3-4; n = 3-4; animal number per group. Mean +/- SEM. **p<0.01, *** p <0.001.

III.6.2. Procoagulant activity of monocyte subsets

To understand the role of different monocyte subsets for immunothrombosis, the subsets were isolated from healthy human blood using FACS sorting. As a next step, TEG was performed in platelet poor plasma (PPP) with PBS (control), C monocytes (PPP+CD14) and NC monocytes (PPP+CD16) (Fig.31).

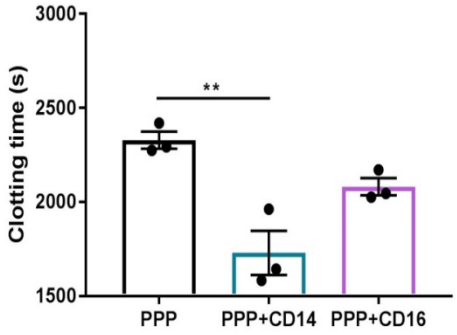

Figure 31: Clotting time of platelet poor plasma without (black) and with (blue, purple) subsets of activated monocytes. n = 3; different experiments. Mean +/- SEM. **p<0.01.

Fig. 31 shows a very low clotting time in samples containing stimulated C monocytes in accordance with a high pro-coagulant activity of these cells. In contrast, activated NC monocytes did not result in a significant increase in fibrin formation.

FXa formation assays were used in addition to TEG to measure the procoagulant activities of monocyte subsets. In this case, both stimulated and unstimulated monocyte subsets were investigated (Fig. 32).

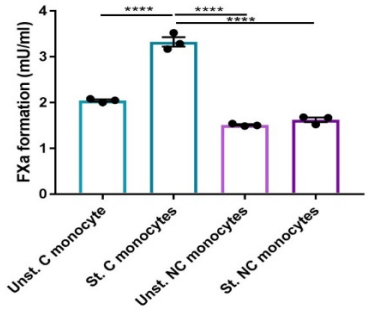

Figure 32: FXa formation by unstimulated C monocytes (column 1), stimulated C monocytes (column 2), unstimulated NC monocytes (column 3) and stimulated NC monocytes (Column 4) n = 3-4; different experiments. Mean +/- SEM. **** p <0.0001.

The high values of FXa formation as induced by stimulated C monocytes confirmed their procoagulant activity compared to both unstimulated C monocytes and NC monocytes. Notably, stimulation of NC monocytes did not increase their ability to enhance factor Xa activation.

III.6.3. Colocalization of NC monocytes with fibrinolytic proteins

In view of these findings we went back to the *in vivo* situation to test whether NC monocytes would present fibrinolytic proteins on their surface that could confirm their coagulant activities.

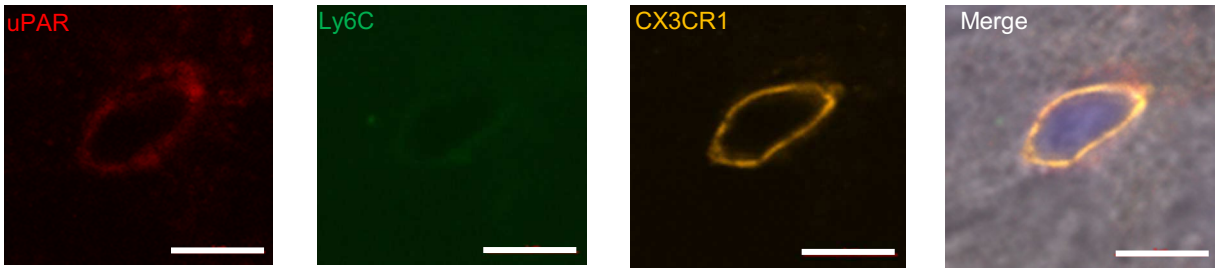

Figure 33: Expression of uPAR on the plasma membrane of NC monocytes after systemic infection with *E.coli* at 6 hr. uPAR was visualized by anti-uPAR antibody (red) on NC monocytes which are negative for Ly6C (green) and positive for CX3CR1 (orange). Scale bar: 5 µm.

Hence, we explored whether NC monocytes presented uPA or uPAR on their membrane surface during systemic infection. Fig. 33 shows that NC monocytes indeed expressed uPAR. Next, the numbers of NC monocytes being positive for uPAR (Fig. 34a) and uPA (Fig. 34b) were counted.

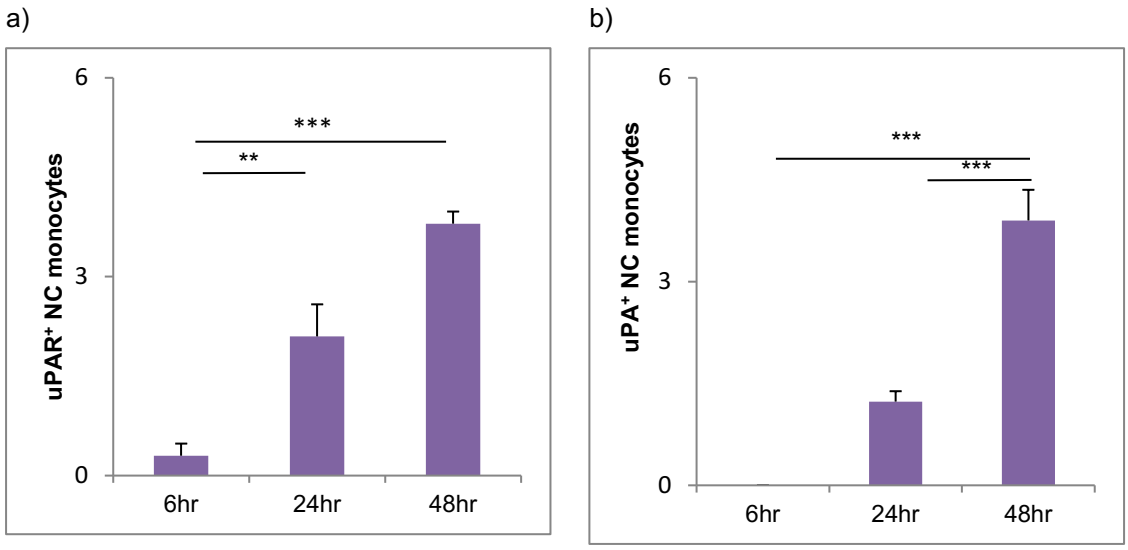

Figure 34: Quantitative analysis of the co-localization of uPAR and uPA with NC monocytes from 6 hr to 48 hr after systemic bacterial infection. n = 3-4; animal number per group. Mean +/- SEM. **p<0.01, *** p < 0.001.

The results show a strong increase in uPAR and uPA positive NC monocytes from 6 hr to 48 hr that suggests a possible role of NC monocytes in fibrinolysis at later stages of the infection process.

III.6.4. Fibrinolytic activities of monocyte subsets

To test the abilities of different monocyte subsets to regulate fibrinolysis both mouse and human monocyte subsets were isolated and submitted to a chromogenic assay, that monitors plasmin activity by calculating the optical density at 405nm.

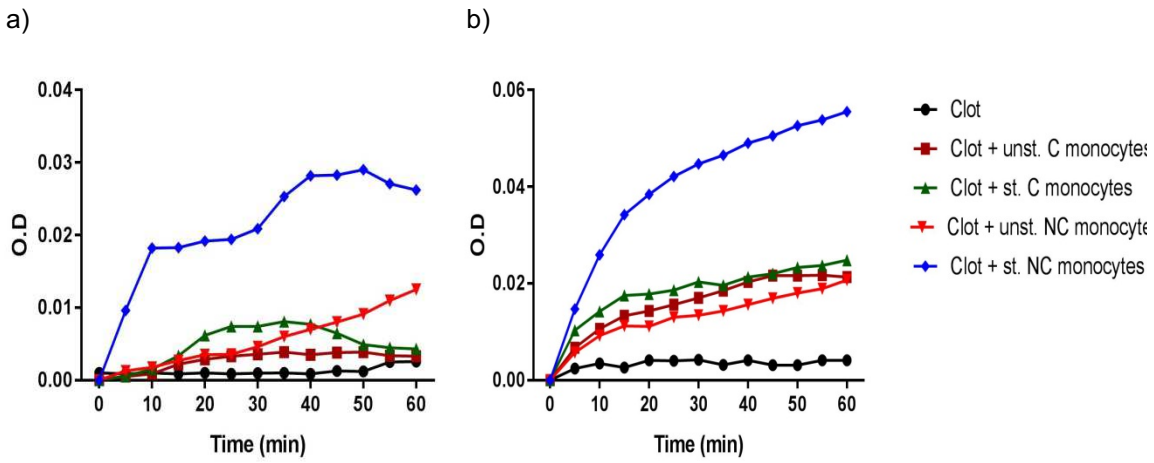

Figure 35: Plasmin activity of monocyte subsets of (a) mouse and (b) human origin. Control without cells; St. NC and C monocytes represent the stimulated NC monocytes and C monocytes respectively, unst. NC and C monocytes represent unstimulated NC monocytes and C monocytes, respectively. Representable of total 3 different experiments.

The results showed that stimulated NC monocytes, but not unstimulated NC monocytes or stimulated or unstimulated C monocyte, strongly support plasmin formation (Fig. 35a, b).

III.6.5. Quantitative PCR

Next, mRNA expression of uPA and uPAR was analyzed in human monocyte subsets. Quantification was based on internal reference genes to determine fold-differences in expression of the target gene.

We observed an increase of the mRNA expression of uPAR and uPA mRNA 2 hr after stimulation of C monocytes and NC monocytes (Fig. 36a, b).

NC monocytes had higher levels of uPA mRNA and of uPAR mRNA as compared to C monocytes. tPA m RNA was almost undetectable in both subtypes (data not shown)

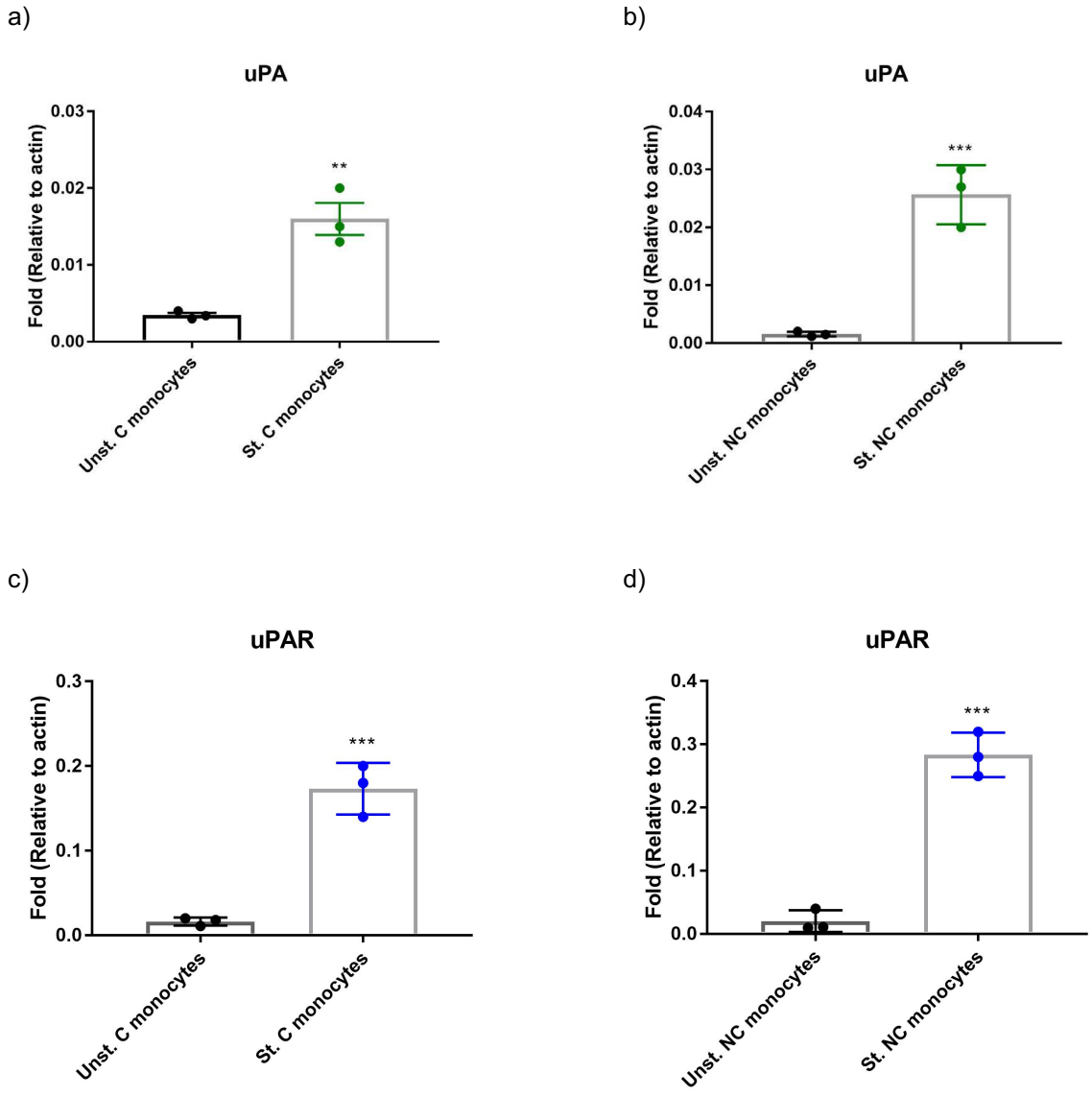

Figure 36: Quantification of gene expression of uPA and uPAR by qPCR in human monocyte subsets. n = 3;different experiments. Mean +/- SEM. **p<0.01, *** p < 0.001.

III.7. MVs and Metastasis

Tumor cells secrete MV that circulate in the blood and may contribute to tumor progression. Here the intravascular immunity response to pancreatic tumor MV and the involvement of vesicles in pancreatic tumor metastasis were investigated.

III.7.1. Characterization of MVs

First, SEM and nanoparticle tracking analyses were performed to check if the isolated tumor vesicles is classified into the category of MVs.

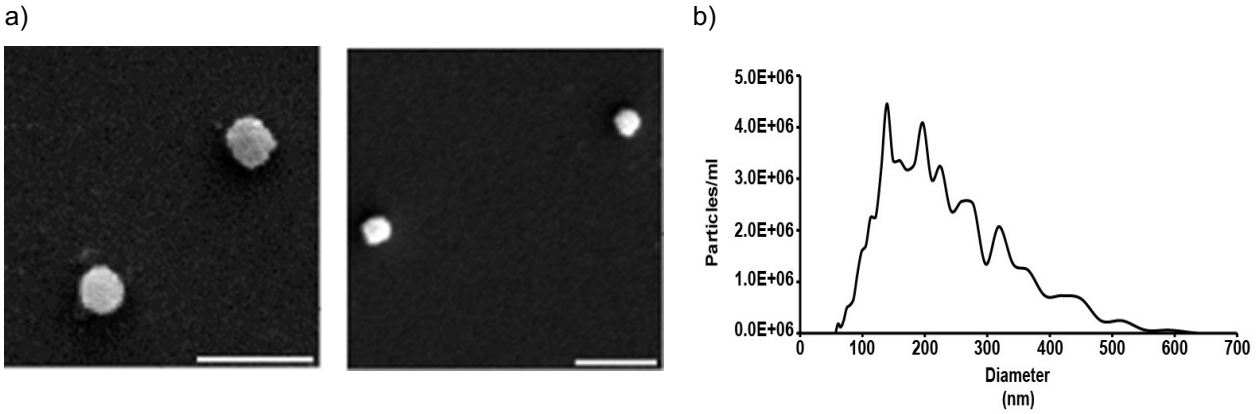

Figure 37: a) SEM of isolated vesicles released from L3.6pl pancreatic tumor cells. Scale bar, 500 nm. (B) Nanoparticle tracking analysis of size (diameter) distributions of isolated L3.6pl vesicles.

SEM image analyses suggested a size of the isolated vesicles in the range of > 0.1 μm and < 0.5 μm (Fig. 37a). Also, the spherical shape was typical of vesicles. Next the size of isolated vesicles was investigated by nanoparticle analyses; thereby it was confirmed that the diameter range of the particles was between 0.1 and 0.5 μm (Fig. 37b).

III.7.2. Interactions of MVs with macrophages *in vitro* and *in vivo*

The interactions of tumor MVs with macrophages *in vitro* were analyzed by using super-resolution microscopy. We were able to visualize separately the intravesicular area and the membrane of the same MV (Fig. 38a) with different markers, DCF for the MV membrane, SYTO RNASelect as well to stain the intravesicular cargo (see Methods). After the incubation of double labelled MV with macrophages intravesicular RNA accumulated in the cytoplasm of the acceptor cells (Fig. 38b). Instead, the membrane marker colocalized with the macrophage cell membrane.

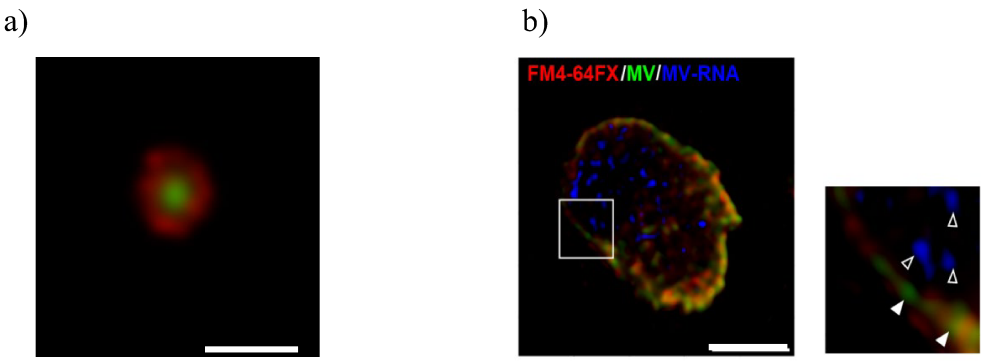

Figure 38: Super resolution image of a) tumor MV labelled with DiD (membrane) and DCF (intravesicular compartment). b) interaction of double labelled tumor MV with macrophages at 60 min. MV membrane, DiD (pseudo-colored,green), intravesicular cargo, RNASelect (pseudo-colored, blue) and macrophage membrane, FM4-64FX (red). Scale bars, 0.5µm.

Next, the internalization of tumor MVs by different type of macrophages in the liver microcirculation at D4, D8 and D14 was analysed *in vivo*. Moreover, the colocalization of MVs with macrophage subtypes was investigated. MVs were present in F4/80^{+}Ly6C^{-} macrophages and only to very small extent in the F4/80^{+}Ly6C^{+} (inflammatory) macrophages (Fig. 39).

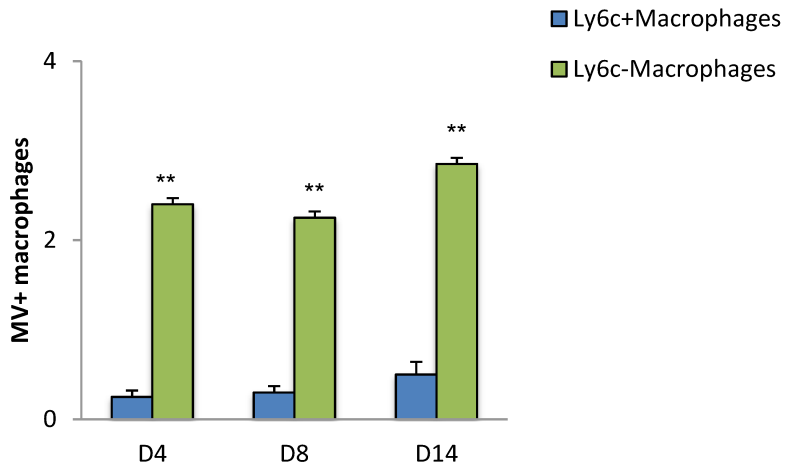

Figure 39: Internalization of tumor MVs by Ly6C^{+} macrophages at D4, D8 and D14. n=3; animals per group. Means +/- SEM. **p<0.01

III.7.3. Role of CD36 for MV internalization into macrophages

To characterize molecular mediators of the cellular uptake of MVs, we investigated the involvement of the class B scavenger CD36. Mice were supplemented with Iso-IgG type antibody or anti-CD36 neutralizing antibody followed by injection of DiD-labelled non-tumor MVs (circulating MVs) and tumor MVs.

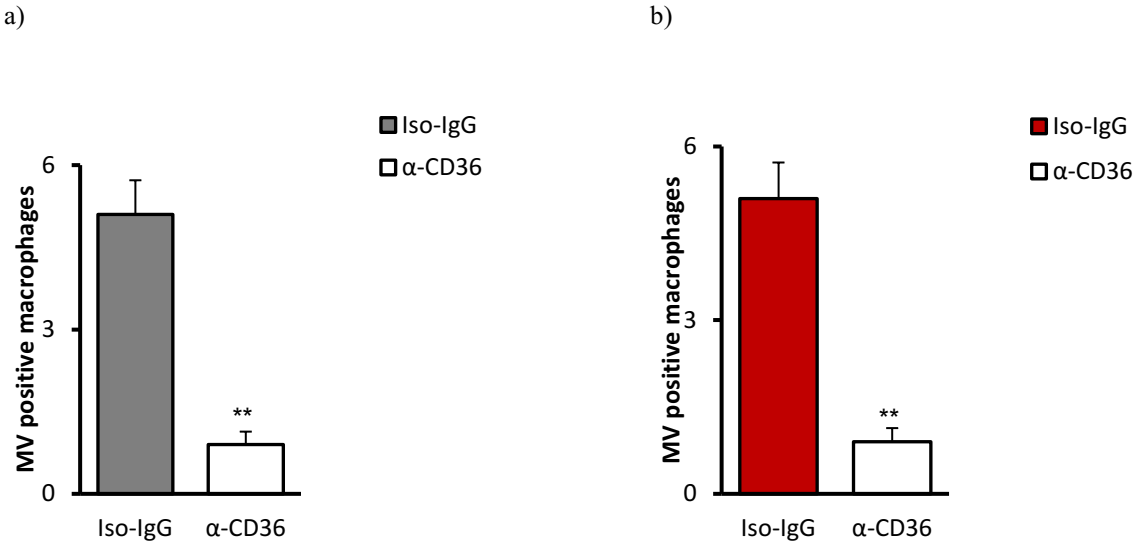

Figure 40: Quantitative analysis of the number of macrophages which engulf a) non-tumor MV and b) tumor MVs. Effect of Iso-IgG control and anti-CD36 neutralization *in vivo*. n = 3, animals per group. Mean +/- SEM ** $p < 0.01$.

In mice infused with Iso-IgG antibody both non-tumor and tumor MVs accumulated in liver macrophages 1 h after MV injection. However, in mice treated with anti-CD36 antibody, MV incorporation by Kupffer cells was almost completely suppressed, suggesting that CD36 strongly contributed to cellular engulfment of non-tumor as well as tumor MVs (Fig. 40a, b).

III.7.4. MV extravasation

We investigated whether MVs were transferred from the intravascular compartment to the perivascular/extravascular tissue. At D0 almost all MVs were localized in intravascular compartment of the liver microcirculation (Fig. 41). Significant increases of MV fluorescence in the tissue occurred at D4, suggesting that the extravasation takes place between D0 and D4 (Fig.41).

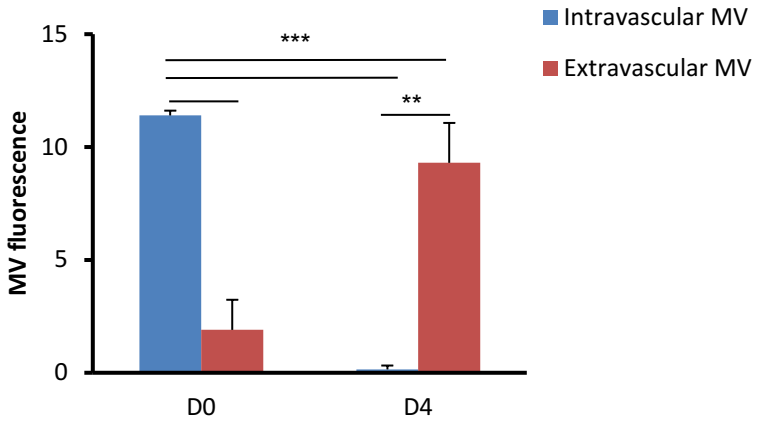

Figure 41: Extravasation of tumor MVs. Quantitative analysis of MV fluorescence present in intravascular space (blue columns) and extravascular tissue (red columns). n = 3; animal number per group. Mean+/- SEM. **p<0.01, *** p < 0.001.

IV. Discussion

In the first part of this thesis, microvascular immunity was analyzed during systemic bacterial infection. Systemic bacterial infection with *E.coli* was used as the main model for inducing intravascular infections, as circulating *E.coli* is a frequent inducer of systemic infections. An unlethal dose of *E.coli* was injected via the tail vein of mice and the infection kinetics was investigated at various time points in the liver and other organs. The rise in bacterial number until the 3 hr time point and a gradually decreasing bacterial survival thereafter suggests a strong efficacy of the intravascular immune system. The liver is known to be an immune-tolerant organ[43] and in accordance with this we found that the survival of *E.coli* in the liver and the spleen was prolonged compared to other organs such as lungs or kidney.

Various cytokines are known to directly or indirectly regulate coagulation and fibrinolysis during systemic infections and related clotting disorders[44]. Since the cytokine MIF plays an important role in systemic inflammatory immune responses, we analyzed its role in immunothrombosis. Previous work with a septic newborn mice, to which a small molecule inhibitor of MIF had been administered suggests that the cytokine can increase bacterial proliferation, systemic immune responses and the mortality of mice[45]. We largely observed similar results with respect to the infection kinetics in E.coli-infected MIF -/- mice, where the presence of MIF increased bacterial survival. Concomitantly, fibrin analyses performed on WT and MIF -/- mice suggested that MIF enhances fibrin formation.

As a next step, to explore how coagulation affects bacterial survival, systemic *E.coli* infection were analyzed in mice with gene deficiency for uPAR and PLG. In uPAR-/- and PLG-/- mice, we observed significant increases in microvascular coagulation and vessel occlusion at 3 hr and 18 hr after infection. . At the same time points the levels of infection was measured in the liver and spleen of uPAR-/- and PLG-/- mice, showing decreased bacterial numbers compared to WT mice. This supports the view that intravascular coagulation supports the inhibition of fibrinolysis and an increased vessel occlusion is associated with an enhanced bacterial killing.

To reveal the pattern of immune cell recruitment upon bacterial infection we analyzed the role of various immune cells in controlling or promoting coagulation in WT mice. Platelets were among the earliest cells to be recruited. Somewhat later (1 hr – 3 hr) $CD4^+$ T cells specifically Th17 cells and NC monocytes appeared (6 hr). The pattern of immune cell recruitment in uPAR-/- and PLG-

/- mice suggest a major impact of fibrin on immune cell recruitment especially the one of Th17 cells and NC monocytes. Based on these results we hypothesized that certain mobile immune cells can serve as counter regulators of immunothrombosis.

The kinetics of appearance of immune cell-associated fibrinolytic proteins suggested a possible role of tPA and PAI-1 at the peak of fibrin formation. As the enzymatic activity of tPA increases from 100-1000 fold upon binding to fibrin[46],[23] the association with the peak of fibrin formation clearly indicates a strong tPA involvement in fibrinolysis at this time point. PAI-1 inhibits tPA and uPA. However, a PAI-1 inhibitor blocks thrombus formation in a mouse model of laser-induced vascular injury[47]. The peak of PAI-1 appearance at 3 hr suggests that it inhibits tPA at this time point and hence contributes to ensure a maximum of fibrin formation.

Next, it was of critical importance to identify the immune cells being associated with fibrinolytic proteins. $CD4^+$ T cells, C monocytes as well as NC monocytes were mostly associated with expressed uPA and uPAR, respectively. These findings encouraged us to uncover a possible role of $CD4^+$ T cells and monocyte subsets during infection. When $CD4^+$ T cells were depleted by neutralizing antibody the bacterial number at both 3 hr and 6 hr post infection were diminished. We next attempted to identify the subtype of $CD4^+$ T cells involved in influencing coagulation. This lead to the characterization of Th17 cells as regulators of fibrin formation.

Th17 cells are believed to be involved in immunity against intracellular bacterial infections induced by *L. monocytogenes*[48], *M. tuberculosis*[49,50], *M. pneumoniae*[51]and *L. donovani*[52]. Translocation of Th17 from gut to kidney has been observed in autoimmune kidney disease[53]. Hence, we hypothesized that during systemic bacterial infection Th17 cells might be translocated from the small intestine to the liver and other organs. To explore a potential recruitment of Th17 cells from the small intestine to the liver during infection photo-convertible Kaede mice were used. To track the Th17 trafficking from the small intestine to other organs, photoconversion was performed and analyzed by Flow cytometry. Flow cytometry analyses of the liver and the lung of infected and non-infected photoconverted Kaede mice suggested their translocation from the small intestine to the liver after 3 hr and 6 hr of infection. Immunofluorescence analyses of Th17 cells in the liver microcirculation pointed to the binding/expression of both fibrinolytic and procoagulant proteins. This, suggested plasticity in their role as regulators of intravascular coagulation as they expressed TF as well as uPA. Moreover, measurements of the plasmin formation activity of different Th17

phenotypes suggested that the anti-inflammatory phenotype of these cells has more fibrinolytic activity as compared to the pro-inflammatory phenotype.

In contrast to C monocytes which were already recruited in the first 1 hr after infection, NC monocytes only appeared 6 hr or later during infection. To understand the potential role of NC monocytes during systemic infection, we determined their procoagulant activity in whole blood (human) and their ability to activate FX. The results show a rather low coagulant activity of NC monocytes as compare to C monocytes in vitro. *In vivo* analyses of uPA- and uPAR- association with immune cells indicated a colocalization with NC monocytes and thus suggested their role in fibrinolysis in the murine liver microcirculation. *In vitro* assays such as the plasmin formation assay supported the conclusion of their role in fibrin degradation. Moreover intravital microscope analyses of CX3CR1-GFP labelled mice suggested uptake of fibrin-coated bacteria by $CX3CR1^{+}$ cells. Altogether, these findings strongly suggest a role of NC monocytes in the degradation of fibrin and of bacterial debris from the liver microcirculation of infected mice.

Fig. 42 summarizes the principle findings of the first part of the thesis in relation to what is known about microvascular immunity in systemic bacterial infection. In the microcirculation of organs such as the liver, which is the site of various metabolic processes as well as site of major immune responses and of immune memory, circulating *E.coli* can be entrapped by microvascular coagulation which might be induced by for example TF expressed by C monocytes (Step I). TF expression especially on C monocytes leads to denser fibrin formation around the bacteria. Then adherent activated platelets enforce the recruitment of neutrophils. In step II, Neutrophil recruitment (as triggered by platelets) and additional immune cells like C monocytes, B1a cells and $CD4^{+}$T cells are attracted. In step III bacteria are potentially killed directly by fibrin as formed around adherent the bacteria and the cytokines released by innate immune cells inside the fibrin clot. In step IV, NC monocytes are recruited together with B cells. NC monocytes may degrade fibrin and clear the bacteria from the circulation.

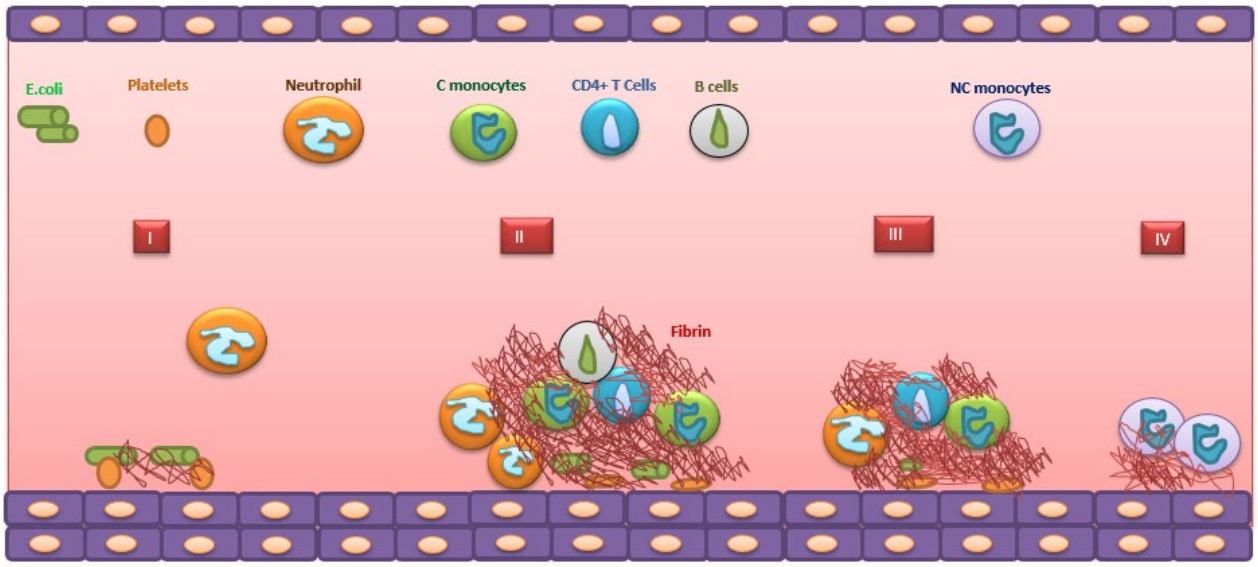

Figure 42: Hypothetical model: Schematic representation of the different steps involved in fibrin generation which mediates microvascular immunity in the liver during systemic bacterial infection. The role of platelets, neutrophils, C monocytes and NC monocytes in the progression of infection are shown. Step (I) involves entrapment of bacteria by fibrin and platelets. During step (II), platelets are activated and neutrophils are recruited together with TF positive C monocytes and $CD4^+$ T cells. (III) Elimination of live bacteria inside the fibrin rich microthrombus. (IV) Clearance of bacterial and host cell debris by NC monocytes from the microcirculation.

In the second part of this work, the interaction of circulating tumor MVs with immune cells was investigated. MVs are generated by release from the plasma membrane through direct budding. Their size varies from 100 to 1000 nm[54,55,56]. Nanoparticle tracking analysis and images generated by using SEM and TEM suggested the spherical shape and diameter range between >0.11 µm and < 0.5 µm which indicated the purity of the isolated MV.

Since tumor MV were rapidly internalized by Kupffer cells *in vivo* we investigated how tumor MV interacted with macrophages *in vitro*. To this purpose, we used super-resolution microscopy to visualize separately for the first time the intravesicular compartment and the vesicle membrane of double labelled MVs. Following incubation of macrophages with tumor MVs, the vesicle membrane colocalized with the plasma membrane of the macrophages. Instead, the MV cargo was delivered to the macrophage cytoplasm. Together this suggested that in contrast to non-tumor MV, tumor MV had fused with the acceptor cell membrane. By delivering different RNA species to the interior of macrophage, the phenotype of the macrophages could be altered so that they might be converted to TAMs. Indeed, it has been reported that melanoma exosomes can promote polarization of M1 to M2 macrophage[57]. In the in vivo experiments extravasation of MVs took

place between days D0 to D4. Most of these MVs had been internalized by perivascular Ly6C$^-$ macrophages at D4 that clearly differ from Kupffer cells. These macrophages could be derived from C monocytes or from recruited NC monocytes[58].

According to the present study CD36 was found to participate in MV extravasation and their internalization by perivascular macrophage which is in line with the finding of a pro-metastatic effect of CD36 in oral cancer[59]. CD36 has also been discussed as a biomarker for metastasis in cancer[60]. Various studies suggest an increased expression of CD36 in human ovarian tumor[61], gastric cancers[62], glioblastoma[63]and oral squamous carcinoma[64].

Our results provide a mechanistic explanation of how CD36 might promote metastasis by showing that CD36 helps tumor MVs to extravasate to foster the formation of the pre-metastatic niche and of macroscopic metastasis.

V. Video links

1. Link

VI. Summary

Intravascular immunity consists of humoral immune responses and cellular immune responses. It involves microvascular coagulation that can entrap circulating bacteria, reduce their dissemination and induce bacterial killing via immunothrombosis. To understand how intravascular coagulation participates in intravascular immunity during systemic bacterial infection we analyzed the immune cell recruitment in response to circulating *E.coli* in the blood stream.

The results show that apart from innate immune cells such as C monocytes and neutrophils there is a massive recruitment of $CD4^+$T cells and B1a cells to the infection sites in the liver microcirculation. By specifying the T helper cell fraction, we found that most of the $CD4^+$T cells were Th17 cells. Next, we investigated the mechanisms involved in counterregulation of immunothrombosis. Here special emphasis was given to the fibrinolytic proteins associated with adherent immune cells during intravascular fibrin formation and to cytokines like MIF that are known to modulate systemic infections. Our findings suggested an important role of MIF for bacterial survival, which might be of relevance for the development of immunothrombosis. In uPAR-/- and PLG-/- mice microvascular coagulation was strongly increased which was associated with reduced bacterial survival. In parallel to this microvascular occlusion was increased substantially. Together this indicated a trade-off between protection from vessel occlusion and microbial killing. Fibrinolytic proteins were mostly associated with Th17 cells and NC monocytes that were recruited in massive amounts during the peak and the resolution of fibrin formation respectively. Systemic infection experiments with Kaede mice suggested a rapid translocation of Th17 cells from the small intestine to the liver microcirculation. The recruitment of NC monocytes during the resolution of fibrin-rich microthrombi intrigued us to find out their specific role in systemic infection. *In vivo* analyses, plasmin activity assays and RT-PCR suggested that these cells possess fibrinolytic properties and could possibly be recruited to clear the fibrin and/or cell debris in the microcirculation.

Since intravascular immunity might be of substantial importance for the outcome of metastasis, we analyze its role in mice challenged with pancreatic tumor microvesicles or tumor cells. EVs were isolated from human and murine pancreatic cell lines and characterized as microvesicles. Interactions of tumor MVs with immune cells were analyzed using *in vitro* and *in vivo* experiments. For the first time nanoscopic imaging was performed to monitor the unique transfer of MV cargo

to immune cells. Upon interaction with macrophages, the vesicle membrane was found to be associated with the cell membrane of the immune cells while the intravesicular cargo especially its RNA cargo, was transferred to the cytosol of the cell. This likely leads to changes in phenotypes of the immune cells consistent with the formation of TAMs. In-vivo experiments suggested the persistence of MVs inside perivascular $Ly6C^-$ macrophages which further participate in the formation of pre metastatic niches. Extravasation of tumor MVs was found to be mediated predominantly by the scavenger receptor CD36. CD36 neutralizing experiments in mice indeed suggested that CD36 promotes invasion of tumor MVs into different types of intravascular or perivascular macrophages.

VII. Zusammenfassung

Die intravaskuläre Immunität setzt sich aus humoralen und zellulären Immunantworten zusammen. Sie beinhaltet auch die mikrovaskuläre Koagulation, welche zirkulierende Bakterien einfangen, deren Ausbreitung eindämmen und via Bildung von Immunothrombosen die Tötung der Bakterien induzieren kann. Um zu verstehen, wie intravaskuläre Koagulation an der intravaskulären Immunität während einer systemischen bakteriellen Infektion mitwirkt, haben wir die Rekrutierung von Immunzellen als Antwort auf zirkulierendes *E.coli* analysiert.

Die Ergebnisse zeigen, dass, abgesehen von Zellen des angeborenen Immunsystems wie beispielsweise klassische Monozyten und Neutrophile, eine massive Rekrutierung von CD4+-T-Zellen und B1a-Zellen in die Mikrozirkulation von infiziertem Gewebe der Leber stattfindet. Durch Spezifizierung der T-Helfer-Zell-Fraktion haben wir herausgefunden, dass der Großteil der CD4+-Zellen Th17-Zellen waren. Daraufhin haben wir die an der Gegenregulation der Immunothrombose beteiligten Mechanismen erforscht. Hierbei lag das Augenmerk vor allem auf den fibrinolytischen Proteinen, die mit adhärierenden Immunzellen während der intravaskulären Fibrinbildung assoziiert waren, und auf Zytokinen, die bekannterweise an der Regulation von Infektionen beteiligt sind, wie MIF. Unsere Ergebnisse ließen auf eine wichtige Rolle des MIF für das Überleben von Bakterien schließen, was für die Bildung der Immunothrombose wichtig sein könnte. In uPAR-/- und PLG-/- Mäusen beobachten wir einen Anstieg der mikrovaskulären Koagulation, der mit einer reduzierten Bakterienzahl assoziiert war. Zudem kam es zu vermehrten mikrovaskulären Gefäßverschlüssen. Zusammengenommen deutet dies auf einen Zielkonflikt zwischen dem Schutz vor Gefäßverschlüssen und der Eliminierung der Pathogene. Fibrinolytische Proteine waren vor allem mit Th17-Zellen und nicht-klassischen Monozyten assoziiert, die auf massive Weise zu den jeweiligen Peaks der Fibrinbildung und -lyse rekrutiert wurden. Experimente mit systemischen Infektionen bei Kaede-Mäusen deuteten auf eine schnelle Translokation von Th17-Zellen aus dem Duenndarm in die Mikrozirkulation der Leber hin. Die Rekrutierung von nicht-klassischen Monozyten während der Lyse von fibrinreichen Mikrothromben hat uns veranlasst, mehr über deren spezifische Rolle in systemischen Infektionen herauszufinden. In vivo-Analysen, Plasmin-Aktivitäts-Messungen und RT-PCR weisen darauf hin, dass diese Zellen starke

fibrinolytische Eigenschaften besitzen und möglicherweise rekrutiert werden, um Fibrin und/oder Zelldebris in der Mikrozirkulation zu beseitigen.

Nachdem die intravaskuläre Immunität von außerordentlicher Bedeutung für den Ausgang von Metastasierung sein könnte, haben wir deren Rolle mithilfe von Mäusen, in die wir Pankreaskarzinomzellen oder deren Mikrovesikel (MV) injiziert haben, analysiert. Die Vesikel wurden aus menschlichen Pankreaskarzinomzelllinien sowie Pankreaskarzinomzelllinien von Mäusen isoliert und als MV charakterisiert. Interaktionen von Tumor-MV mit Immunzellen wurden sowohl mittels *in vitro*- als auch *in vivo*-Experimenten nachgewiesen. Zum ersten Mal wurden nanoskopische Aufnahmen durchgeführt, um den einzigartigen Transfer von MV-Cargo in Immunzellen zu beobachten. Es stellte sich heraus, dass sich infolge der Interaktion mit Makrophagen die Membran der Vesikel mit der Zellmembran der Immunzellen verbindet, während der Inhalt, besonders die RNA, in das Zytosol der Zelle transferiert wird. Dies führt möglicherweise zu Veränderungen im Phänotyp der Immunzellen und infolgedessen zur Bildung von TAMs. *In vivo*-Experimente zeigen das Verbleiben der MV innerhalb von perivaskulären Ly6C- Makrophagen, welche daraufhin an der Bildung von prämetastatischen Nischen beteiligt sind. Wir haben außerdem herausgefunden, dass die Extravasation von Tumor-MV vor allem durch den Scavenger-Rezeptor CD36 herbeigeführt wird. CD36-neutralisierende Experimente mit Mäusen lassen in der Tat darauf schließen, dass CD36 die Invasion von Tumor-MV in verschiedene Typen von intravaskulären oder perivaskulären Makrophagen begünstigt.

VIII. References

1. Iwasaki, A. & Medzhitov, R. Regulation of adaptive immunity by the innate immune system. *Science* **327**, 291–5 (2010).

2. Broz, P. & Monack, D. M. Newly described pattern recognition receptors team up against intracellular pathogens. *Nat. Rev. Immunol.* **13**, 551–565 (2013).

3. Fleischmann, C. *et al.* Assessment of global incidence and mortality of hospital-treated sepsis current estimates and limitations. *Am. J. Respir. Crit. Care Med.* **193**, 259–272 (2016).

4. Casadevall, A., Dadachova, E. & Pirofski, L. A. Passive antibody therapy for infectious diseases. *Nat. Rev. Microbiol.* **2**, 695–703 (2004).

5. Menny, A. *et al.* CryoEM reveals how the complement membrane attack complex ruptures lipid bilayers. *Nat. Commun.* **9**, 5316 (2018).

6. Shao, Z., Nishimura, T., Leung, L. L. K. & Morser, J. Carboxypeptidase B2 Deficiency Reveals Opposite Effects of Complement C3a and C5a in a Murine Polymicrobial Sepsis Model. *J Thromb Haemost.* **6**,1090-102 (2015).

7. Silasi-Mansat, R. *et al.* Complement inhibition decreases the procoagulant response and confers organ protection in a baboon model of Escherichia coli sepsis. *Blood* **116**, 1002–10 (2010).

8. Papayannopoulos, V. Neutrophil extracellular traps in immunity and disease. *Nat. Rev. Immunol.* **18**, 134–147 (2017).

9. Ramirez, G. A., Rovere-Querini, P., Sabbadini, M. G. & Manfredi, A. A. Parietal and intravascular innate mechanisms of vascular inflammation. *Arthritis Res. Ther.* **17**, 16 (2015).

10. Kapoor, S., Opneja, A. & Nayak, L. The role of neutrophils in thrombosis. *Thromb. Res.* **170**, 87–96 (2018).

11. Pfeiler, S., Massberg, S. & Engelmann, B. Biological basis and pathological relevance of microvascular thrombosis. *Thromb. Res.* **133**, S35–S37 (2014).

12. Sampath, P., Moideen, K., Ranganathan, U. D. & Bethunaickan, R. Monocyte Subsets: Phenotypes and Function in Tuberculosis Infection. *Front. Immunol.* **9**, 1726 (2018).

13. Geissmann, F. *et al.* Blood monocytes: distinct subsets, how they relate to dendritic cells, and their possible roles in the regulation of T-cell responses. *Immunol. Cell Biol.* **86**, 398–408 (2008).

14. Carlin, L. M. *et al.* Nr4a1-Dependent Ly6Clow Monocytes Monitor Endothelial Cells and Orchestrate Their Disposal. *Cell* **153**, 362–375 (2013).

15. Flannagan, R. S., Cosío, G. & Grinstein, S. Antimicrobial mechanisms of phagocytes and bacterial evasion strategies. *Nat. Rev. Microbiol.* **7**, 355–366 (2009).

16. Flannagan, R. S., Kuiack, R. C., McGavin, M. J. & Heinrichs, D. E. Staphylococcus aureus Uses the GraXRS Regulatory System To Sense and Adapt to the Acidified Phagolysosome in Macrophages. *MBio* **9**:e01143-18 (2018).

17. Hickey, M. J. & Kubes, P. Intravascular immunity: the host-pathogen encounter in blood vessels. *Nat. Rev. Immunol.* **9**, 364–75 (2009).

18. Versteeg, H. H., Heemskerk, J. W. M., Levi, M. & Reitsma, P. H. New Fundamentals in Hemostasis. *Physiol. Rev.* **93**, 327–358 (2013).

19. Wolberg, A. S. Thrombin generation and fibrin clot structure. *Blood Rev.* **21**, 131–142 (2007).

20. Aleman, M. M., Walton, B. L., Byrnes, J. R. & Wolberg, A. S. Fibrinogen and red blood cells in venous thrombosis. *Thromb. Res.* **133**, S38–S40 (2014).

21. Esmon, C. T. The interactions between inflammation and coagulation. *Br. J. Haematol.* **131**, 417–430 (2005).

22. Jen, C. J. & McIntire, L. V. The structural properties and contractile force of a clot. *Cell Motil.* **2**, 445–55 (1982).

23. Hudson, N. E. Biophysical Mechanisms Mediating Fibrin Fiber Lysis. *Biomed Res. Int.* **2017**, 2748340 (2017).

24. Kollman, J. M., Pandi, L., Sawaya, M. R., Riley, M. & Doolittle, R. F. Crystal Structure of Human Fibrinogen. *Biochemistry* **48**, 3877–3886 (2009).

25. Massberg, S. *et al.* Reciprocal coupling of coagulation and innate immunity via neutrophil serine proteases. *Nat. Med.* **16**, 887–896 (2010).

26. Brinkmann, V. *et al.* Neutrophil Extracellular Traps Kill Bacteria. *Science.* **303**, 1532–1535 (2004).

27. Engelmann, B. & Massberg, S. Thrombosis as an intravascular effector of innate immunity. *Nat. Rev. Immunol.* **13**, 34–45 (2013).

28. Longstaff, C. & Kolev, K. Basic mechanisms and regulation of fibrinolysis. *J. Thromb. Haemost.* **13**, S98–S105 (2015).

29. Chapin, J. C. & Hajjar, K. A. Fibrinolysis and the control of blood coagulation. *Blood Rev.* **29**, 17–24 (2015).

30. Rijken, D. C. & Uitte de Willige, S. Inhibition of Fibrinolysis by Coagulation Factor XIII. *Biomed Res. Int.* **2017**, 1–6 (2017).

31. Silva, M. M. C. G., Thelwell, C., Williams, S. C. & Longstaff, C. Regulation of fibrinolysis by C-terminal lysines operates through plasminogen and plasmin but not tissue-type plasminogen activator. *J. Thromb. Haemost.* **10**, 2354–60 (2012).

32. van der Poll, T. & Herwald, H. The coagulation system and its function in early immune defense. *Thromb. Haemost.* **112**, 640–648 (2014).

33. Maas, S. L. N., Breakefield, X. O. & Weaver, A. M. Extracellular Vesicles: Unique Intercellular Delivery Vehicles. *Trends Cell Biol.* **27**, 172–188 (2017).

34. Pan, Q. *et al.* Microvesicles-mediated communication between endothelial cells modulates, endothelial survival, and angiogenic function via transferring of miR-125a-5p. *J. Cell. Biochem.* **120,** 3160-3172. (2019).

35. Muralidharan-Chari, V., Clancy, J. W., Sedgwick, A. & D'Souza-Schorey, C. Microvesicles: mediators of extracellular communication during cancer progression. *J. Cell Sci.* **123**, 1603–1611 (2010).

36. Eyles, J. *et al.* Tumor cells disseminate early, but immunosurveillance limits metastatic outgrowth, in a mouse model of melanoma. *J. Clin. Invest.* **120**, 2030–9 (2010).

37. Paolino, M. *et al.* The E3 ligase Cbl-b and TAM receptors regulate cancer metastasis via natural killer cells. *Nature* **507**, 508–12 (2014).

38. Fusella, F., Seclì, L. & Brancaccio, M. Escaping NK cells and recruiting neutrophils: How Morgana/NF-κB signaling promotes metastasis. *Mol. Cell. Oncol.* **5**, e1432258 (2018).

39. Liu, Y. & Cao, X. Immunosuppressive cells in tumor immune escape and metastasis. *J. Mol. Med.* **94**, 509–522 (2016).

40. Kitamura, T., Qian, B.-Z. & Pollard, J. W. Immune cell promotion of metastasis. *Nat. Rev. Immunol.* **15**, 73–86 (2015).

41. Qian, B.-Z. & Pollard, J. W. Macrophage diversity enhances tumor progression and metastasis. *Cell* **141**, 39–51 (2010).

42. Noy, R. & Pollard, J. W. Tumor-Associated Macrophages: From Mechanisms to Therapy. *Immunity* **41**, 49–61 (2014).

43. Kubes, P. & Jenne, C. Immune Responses in the Liver. *Annu. Rev. Immunol.* **36**, 247–277 (2018).

44. Low, C. *et al.* Modulation of Interleukins in Sepsis-Associated Clotting Disorders. *Clin. Appl. Thromb.* **23**, 34–39 (2017).

45. Roger, T. *et al.* High expression levels of macrophage migration inhibitory factor sustain the innate immune responses of neonates. *Proc. Natl. Acad. Sci. U. S. A.* **113**, E997-1005 (2016).

46. Hoylaerts, M., Rijken, D. C., Lijnen, H. R. & Collen, D. Kinetics of the activation of plasminogen by human tissue plasminogen activator. Role of fibrin. *J. Biol. Chem.* **257**,

2912–9 (1982).

47. Peng, S. *et al.* A long-acting PAI-1 inhibitor reduces thrombus formation. *Thromb. Haemost.* **117**, 1338–1347 (2017).

48. Orgun, N. N., Mathis, M. A., Wilson, C. B. & Way, S. S. Deviation from a strong Th1-dominated to a modest Th17-dominated CD4 T cell response in the absence of IL-12p40 and type I IFNs sustains protective CD8 T cells. *J. Immunol.* **180**, 4109–15 (2008).

49. Paidipally, P. *et al.* NKG2D-Dependent IL-17 Production by Human T Cells in Response to an Intracellular Pathogen. *J. Immunol.* **183**, 1940–1945 (2009).

50. Umemura, M. *et al.* IL-17-mediated regulation of innate and acquired immune response against pulmonary Mycobacterium bovis bacille Calmette-Guerin infection. *J. Immunol.* **178**, 3786–96 (2007).

51. Wu, Q. *et al.* IL-23-dependent IL-17 production is essential in neutrophil recruitment and activity in mouse lung defense against respiratory Mycoplasma pneumoniae infection. *Microbes Infect.* **9**, 78–86 (2007).

52. Pitta, M. G. R. *et al.* IL-17 and IL-22 are associated with protection against human kala azar caused by Leishmania donovani. *J. Clin. Invest.* **119**, 2379–87 (2009).

53. Krebs, C. F. *et al.* Autoimmune Renal Disease Is Exacerbated by S1P-Receptor-1-Dependent Intestinal Th17 Cell Migration to the Kidney. *Immunity* **45**, 1078–1092 (2016).

54. György, B. *et al.* Membrane vesicles, current state-of-the-art: emerging role of extracellular vesicles. *Cell. Mol. Life Sci.* **68**, 2667–2688 (2011).

55. Cocucci, E., Racchetti, G. & Meldolesi, J. Shedding microvesicles: artefacts no more. *Trends Cell Biol.* **19**, 43–51 (2009).

56. Piccin, A., Murphy, W. G. & Smith, O. P. Circulating microparticles: pathophysiology and clinical implications. *Blood Rev.* **21**, 157–171 (2007).

57. Bardi, G. T., Smith, M. A. & Hood, J. L. Melanoma exosomes promote mixed M1 and M2 macrophage polarization. *Cytokine* **105**, 63–72 (2018).

58. Krenkel, O. & Tacke, F. Liver macrophages in tissue homeostasis and disease. *Nat. Rev. Immunol.* **17**, 306–321 (2017).

59. Enciu, A.-M., Radu, E., Popescu, I. D., Hinescu, M. E. & Ceafalan, L. C. Targeting CD36 as Biomarker for Metastasis Prognostic: How Far from Translation into Clinical Practice? *Biomed Res. Int.* **2018**, 7801202 (2018).

60. Enciu, A.-M., Radu, E., Popescu, I. D., Hinescu, M. E. & Ceafalan, L. C. Targeting CD36 as Biomarker for Metastasis Prognostic: How Far from Translation into Clinical Practice? *Biomed Res. Int.* **2018**, 7801202 (2018).

61. Ladanyi, A. *et al.* Adipocyte-induced CD36 expression drives ovarian cancer progression and metastasis. *Oncogene* **37**, 2285–2301 (2018).

62. Kashihara, H. *et al.* Correlation Between Thrombospondin-1 Expression in Non-cancer Tissue and Gastric Carcinogenesis. *Anticancer Res.* **37**, 3547–3552 (2017).

63. Hale, J. S. *et al.* Cancer Stem Cell-Specific Scavenger Receptor CD36 Drives Glioblastoma Progression. *Stem Cells* **32**, 1746–1758 (2014).

64. Pascual, G. *et al.* Targeting metastasis-initiating cells through the fatty acid receptor CD36. *Nature* **541**, 41–45 (2017).

VIII. Acknowledgement

First, I would like to express my heartiest thanks to Prof. Dr. med. Bernd Engelmann for giving me the opportunity to work in his group as a PhD. I am highly obliged to him for assisting me at every step of entire course of my experimental work, his positive criticism to bring out the best in me as well as for his careful and accurate correction of my written thesis. I deeply thank him for being patient with me and giving me his expert guidance and constant motivation to help me excel in my scientific career.

Next, I would like to thank Prof. Dr. med. Daniel Teupser, the director of the Institut für Laboratoriumsmedizin, Klinikum der Universität München, Ludwig-Maximilians-Universität (LMU) for allowing me to conduct my research work.

I am very grateful to all my lab mates and colleagues for a wonderful time in the lab. Susi for her constant supervision and advice with research as well as with using various programs and advice regarding presenting my data, a very special thanks to Ana (Chinnu), Urjita, Raphael, Leni and Lydia for all their encouragement in work, life and as well for keeping joyful environment in the lab. Thanks to Lena and Mona for the mint motivation and especially Lena for helping me with German translations. Thanks to Sarah, Tonina, Flavio and Pia for all their hard work and individual contribution to take the project further. I would also like to thank my colleagues from the old lab: Mr. Wolfgang, Andreas, Alex, Anika and Bernd for helping me with certain experiments and machines.

I would further like to thank Prof. Dr. med. Steffen Massberg (Medizinische Klinik und Poliklinik I, Klinikum der Universität München) and his working group for their highly valuable collaboration.

Prof. Dr. med. Christian Schulz, Mrs. Ana Titova, for their highly valuable co-operation and for providing their expertise particularly for all FACS. Dr. Hellen Ishikawa-Ankerhold, Dr. med. Konstantin Stark and Dr. med. Vet. Meike Miller for helping with animal experiments and training.

I would also like to thank Prof. Dr. med. Christian Weber (IPEC, LMU Munich) for unwavering support and collaboration; Dr. Remco T.A. Megens for his kind help Regarding STED and Dr. Philipp von Hundelshausen.

Furthermore, I would like to thank our co-operation partners Prof. Dr. med. Samuel Huber (UKE, Hamburg), especially Laura and Tasos for their help with experiments on Kaede mice and Th17 cells. I would also like to thank our collaborators Prof. Dr. Karen Vanhoorelbeke (KU Leuven), Prof. Andreas Klingl for helping with electron microscope, Prof. Dr. Jürgen Bernhagen for providing different animals models vital for the project.

Apart from that, I cannot thank enough my mother Meera Thakur and my brother Dhiraj Thakur for their unconditional love, emotional support and their belief in my skills and abilities. I dedicate my doctoral thesis to them. I am thankful to all my friends here in Germany, Switzerland, U.S and India especially Tilak and Bhavuk for guiding me to get started in research. Finally yet importantly, I am grateful to almighty Universe for throwing fascinating opportunities on my way and making me excel in scientific research and life.

X. Publications related to the thesis

1. Pfeiler, Susanne*, **Manovriti Thakur***, Petra Grünauer, Remco T. A. Megens, Urjita Joshi, Raffaele Coletti, Verena Samara, Geraldine Müller-Stoy, Hellen Ishikawa-Ankerhold, Konstantin Stark, Andreas Klingl, Thomas Fröhlich, Georg J. Arnold, Sonja Wörmann, Christiane J. Bruns, Hana Algül, Christian Weber, Steffen Massberg, and Bernd Engelmann. 2019. "CD36-Triggered Cell Invasion and Persistent Tissue Colonization by Tumor Microvesicles during Metastasis." *FASEB J 33(2):1860-1872.*

* Contributed equally

2. Stark, Konstantin, Irene Schubert, Urjita Joshi, Badr Kilani, Parandis Hoseinpour, **Manovriti Thakur**, Petra Grünauer, Susanne Pfeiler, Tobias Schmidergall, Sven Stockhausen, Markus Bäumer, Sue Chandraratne, Marie-Luise von Brühl, Michael Lorenz, Raffaele Coletti, Sven Reese, Iina Laitinen, Sonja Maria Wörmann, Hana Algül, Christiane J. Bruns, Jerry Ware, Nigel Mackman, Bernd Engelmann, and Steffen Massberg. 2018. "Distinct Pathogenesis of Pancreatic Cancer Microvesicle–Associated Venous Thrombosis Identifies New Antithrombotic Targets In Vivo." *Arteriosclerosis, Thrombosis, and Vascular Biology* 38(4):772–86.

LMU LUDWIG-MAXIMILIANS-UNIVERSITÄT MÜNCHEN

Dean's Office
Faculty of Medicine

MMRS

Affidavit

Thakur, Manovriti

Surname, first name

-

Street

-

Zip code, town

-

Country

I hereby declare, that the submitted thesis entitled

Intravascular immunity against systemic bacterial infection and metastasis.

is my own work. I have only used the sources indicated and have not made unauthorised use of services of a third party. Where the work of others has been quoted or reproduced, the source is always given.

I further declare that the submitted thesis or parts thereof have not been presented as part of an examination degree to any other university.

Munich, 22.07.2018 Manovriti thakur

Place, date

Signature doctoral candidate